REC-ERC-88-3

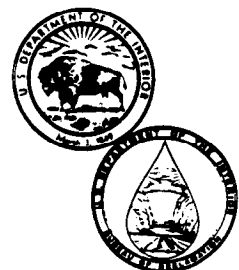# OVERTOPPING FLOW ON LOW EMBANKMENT DAMS —SUMMARY REPORT OF MODEL TESTS

Denver Office
August 1988

U. S. Department of the Interior

Bureau of Reclamation

TECHNICAL REPORT STANDARD TITLE PAGE

1. REPORT NO. REC-ERC-88-3	2. GOVERNMENT ACCESSION NO.	3. RECIPIENT'S CATALOG NO.
4. TITLE AND SUBTITLE Overtopping Flow on Low Embankment Dams — Summary Report of Model Tests		5. REPORT DATE August 1988
		6. PERFORMING ORGANIZATION CODE D-1531
7. AUTHOR(S) R. A. Dodge		8. PERFORMING ORGANIZATION REPORT NO. REC-ERC-88-3
9. PERFORMING ORGANIZATION NAME AND ADDRESS Bureau of Reclamation Denver Office Denver, Colorado		10. WORK UNIT NO.
		11. CONTRACT OR GRANT NO.
12. SPONSORING AGENCY NAME AND ADDRESS Same		13. TYPE OF REPORT AND PERIOD COVERED
		14. SPONSORING AGENCY CODE DIBR

15. SUPPLEMENTARY NOTES
Microfiche and/or hard copy available at the Denver Office, Denver, Colorado Ed:RNW

16. ABSTRACT

A 1:15 scale model was used to study the relative effectiveness of different embankment protective treatments. Tests were done representing unit discharges of 40 and 86 ft³/s. Chute and pool mode flow occurred for all treatments tested. Chute and pool flow had less scouring power compared with the earlier less rough plane flow. A smooth hard crest cap going part way down the slope caused a deep scour hole just downstream of the cap. The same flow, after roughening the sloping part of the cap with epoxied pea gravel simulating fixed cobble roughness, scoured one-half the volume compared with plain cap test. Riprap, with a simulated maximum size of 24 inches, immediately fluidized and washed out completely. There was no indication that any of the mesh-contained treatments would fail. Flow on an embankment slope of 4:1, protected by gabbions scoured 2.5 times the volume for a gabbion protected 1:6 slope. A change of compaction from 95 to 102 percent standard Proctor density decreased scour one-half. Doubling the unit discharge increased scour by a factor of 1.4 times. Both design and modeling are hampered by lack of sufficiently verified equations for steep flow and for chute and pool flow. Therefore these test results are relative and future research is suggested.

17. KEY WORDS AND DOCUMENT ANALYSIS

a. DESCRIPTORS-- hydraulic models/ *overtopping flow/ embankments/ *erosion/ low dams/ *bank protection/ plain soil/ extended crest caps/ roughened cap/ gabbions/ rock mattress/ riprap

b. IDENTIFIERS-- Blue Ridge Parkway Dam/

c. COSATI Field/Group 08M   COWRR: 0813   SRIM:

18. DISTRIBUTION STATEMENT	19. SECURITY CLASS (THIS REPORT) UNCLASSIFIED	21. NO. OF PAGES 28
Available from the National Technical Information Service, Operations Division, 5285 Port Royal Road, Springfield, Virginia 22161.	20. SECURITY CLASS (THIS PAGE) UNCLASSIFIED	22. PRICE

OVERTOPPING FLOW ON LOW EMBANKMENT DAMS — SUMMARY REPORT OF MODEL TESTS

by
R. A. Dodge

August 1988

ACKNOWLEDGMENTS

CONTENTS

CONTENTS — Continued

LETTER SYMBOLS AND QUANTITIES

A — Area of flow section

A_c — Flow area of the critical depth flow section or control section

A_w — Wetted area that forces flow between roughness elements

ΔA_c — Incremental flow area at control station

C_o — Dimensionless cohesion, function of some combination of soil parameters

$\%C$ — Percent clay in a soil

C_s — Compressive strength

c — Subscript denoting soil compaction

c — Subscript denoting characteristic or boundary value

C — Chezy coefficient

d — Sediment diameter or differential operator

d_i — d is sediment diameter where i equals (or less than) 50, 90, or 100 percentage of the sediment weight (mass) finer than that diameter

$\bar{D}$ — Mean depth of flow reach

D — Depth of flow section

D_c — Flow depth at control section

D_1 — Approach flow depth

D_* — Dimensionless flow depth

e — Base of natural logrithm, 2.71828 . . .

e — Soil voids ratio

e — Subscript denoting erosion

f — Darcy Weisbach friction factor

f_s — Steep flow and large element roughness friction factor

f_t — Friction factor at threshold of sediment motion

F — Froude number, $4R_hV/\nu$ or $V_c/g^{1/2}x^{1/2}$

g — Gravitational constant (acceleration)

h_f — Friction head loss

H — head

H_c — Head at critcal or control section

H_1 — Approach head

k — Dimensional erosion constant, same units as sediment discharge

K_d — Skewness of sediment size distribution

k_s — Rugosity, boundary surface roughness

k_m — A mass erodiability constant

k_v — A volume erosion constant

k_e — An erosion constant

l — Subscript denoting level

L — Crest length

L_r — Model length scale ratio

m — Subscript denoting mass

n — Manning's coefficient

n — An exponent

N — Dimensionless parameter

o — Subscript denoting boundary value

P — Flow section wetted perimeter

P_c — Soil density compaction parameter

q — Discharge per unit width

q_r — Unit discharge ratio

q_{sm} — Unit mass sediment discharge

q_s — Sediment discharge in volume per unit width per second. (In Taylor's dimensionless discharge parameter or defined by units used in other empirical equation for cohesive transfer)

q_{s*} — Dimensionless unit volume discharge

q_{sv} — Unit volume sediment discharge

Q — Water discharge

R — Reynolds number $4Vr/\nu$

R_{*g} — Shear velocity grain diameter Reynolds number, U_*d/ν

R_h — Hydraulic radius, A/P

R_{ht}	Hydraulic radius at threshold of sediment motion
R_r	Reynolds number distortion ratio
s	Subscript denoting sediment
S	Slope, horizontal to vertical
S_{sv}	Vane shear strength
S_t	Slope of energy gradient at threshold of sediment motion
T_c	Top width of flow at control section
T_r	Time scale ratio
U_*	Shear velocity
U_{*t}	Shear velocity at threshold of sediment movement
v_c	Velocity of incremental area of control section
V	Average flow velocity
V_c	Characteristic average velocity of flow
V_l	Average velocity on a level bed
V_r	Velocity scale ratio
V_s	Average velocity on a dam or canal bank
V_t	Velocity at threshold of sediment motion
V_*	Dimensionless velocity
v_1	Velocity at distance of y_1 above bed
v_2	Velocity at distance y_2 above bed
V'	Velocity fluctuation
W	Width of rough element flow section
w	Subscript denoting water
X	Distance along flow slope
X_c	Characteristic distance along flow slope
X_*	Dimensionless distance along flow slope
y_1	A distance above bed below y_2
y_2	A distance above bed above y_1
Z	Distance of flow bed above elevation datum
α	Velocity distribution coefficient or kinetic energy correction factor
α_c	Control section velocity distribution coefficient
α_1	Measuring head section velocity distribution coefficient
β	Angle of flow relative to a horizontal line in the plane of canal side slope
γ	Specific weight of water, density times gravitational constant
Δ	Small increment
ε_t	Turbulent intensity
θ	Angle of repose for bank material
λ	Roughness concentration parameter, a function of spacing, distribution roughness elements, and element size relative to depth of flow
μ	Subscript denoting mean
ν	Kinematic viscosity
ρ	Density of water
ρ_s	Density of sediment
τ	Tractive shear on flow bed
σ	Standard deviation of grain size distribution
τ_1	Tractive shear on level bed
τ_s	Tractive shear on sloping bank
τ_t	Tractive shear at threshold of sediment motion
τ_*	Dimensionless tractive shear
φ	Slope angle canal side bank or dam embankment
Φ	Function operator

INTRODUCTION

Purpose of the Model Study

The investigations were to determine, with a sectional model, the modes of flow and the erosion on downstream slope protection for small embankment dams during overtopping flow. Model experience will greatly aid to determine model scales and capability, and to decide whether further physical model studies are feasible. The results will be used to evaluate future research needs. These model results can be used to help form concepts for treating existing small embankment dams so they can possibly overtop resulting from the larger design flows that have been determined by contemporary flood routing methods. The studies were supported by the Bureau of Reclamation Dam Safety Program concerning overtopping flow on low embankment dams.

Background

It is assumed that when an embankment dam is overtopped, erosion on the downstream slope and toe of the dam will lead to embankment failure. Consequently, overtopping is not permitted by contemporary design.

The PMF (probable maximum flood) has been used by the Bureau of Reclamation [1]* as the IDF (inflow design flood) for new dam designs and for modification of existing dams when failure could cause potential loss of human life or significant property damage. Because of larger predicted storms using the current data base, the PMS (probable maximum storm) and PMF magnitudes used for design of new dams and modification of existing dams have increased significantly. By this criteria, many existing small embankment dams need increased spillway capacity or require greater dam height to eliminate overtopping. When designing new dams and spillways or modifying existing dams to meet revised restrictions—and often larger PMF—costs can become excessive. In some instances, it may not be physically nor economically feasible to accommodate large floods without overtopping. In fact, some embankment dams have been removed rather than undergo exorbitant costs of modification. However, some embankments have undergone moderate overtopping without failure [2]. Therefore, it is surmised some existing embankment dams, especially those less than 50 feet (15.24 m) high, could possibly be modified to safely permit overtopping.

CONCLUSIONS

Conclusion Based on Model Tests

The conclusions here are based upon observations of single tests. At the current state of technology,

conclusions should be considered relative to each other; i.e., the model—aside from lack of repeated tests—is expected only to determine which of the treatments tested worked better, but not actually how much better. These conclusions are also specific to the single soil tested. With these limits in mind, it is concluded that:

1. For all treatments tested, flow eventually transformed into chute and pool mode.

2. Chute and pool flow had less scouring power compared with the less-rough plane shear flow, which occurred earlier.

3. The smooth hard crest cap extending 10 feet (3.048 m) down the slope caused a deep scour hole just downstream of the cap.

4. The flow, after roughening the sloping part of the cap with epoxied pea gravel—representing fixed cobble roughness, scoured out one-half the embankment volume compared to erosion with the smooth hard crest cap.

5. Riprap, with a simulated maximum size of 24 inches (610 mm), immediately fluidized and washed out.

6. The mesh-contained treatments tested showed no indication of failure.

7. Flow on the embankment slope of 4:1, protected with gabions, scoured five times the volume compared to the gabion protected 6:1 slope.

8. A change of compaction from 95 to 102 percent standard Proctor density decreased volume of scour by one-half.

9. Scour increased about 40 percent by doubling the unit discharge from 40 to 87 (ft³/s)/ft [3.716 to 8.082 (m³/s)/m].

10. A slight sag any place along a crest axis combined with a slowly rising hydrograph can cause gully-type erosion and eventual breaching.

11. Flow, with approach head less than about one-twelfth of the crest length in the direction of the flow, will cause undulating flow on the crest; i.e., attempting to pass through critical depth more than once.

12. Design predictions are hampered by lack of verified adequate governing equations for flow and sediment entrainment and transport for the steep shallow case.

---

* Number in brackets refer to the bibliography.

13. Reservoir pool geometry can cause side and centrally located bottom eddies that will be intensified longitudinally by upstream embankment uplift into strong sediment transporting vortices downstream from the crest.

Conclusions Related to Modeling and Design Needs

The following conclusions are based on literature review and analyses. Some analyses are based on proposed equations and relationships that are not fully verified nor modified and/or tested for steep ($\tan\varphi$ greater than 0.08) and shallow ($k_s/4D$ greater than 0.1) flow. However, this analysis suggests possible research approaches. The conclusions also reflect design and modeling needs; they should help in the decision process for planning and monitoring possible future Bureau investigations or contract research.

1. Suitable flow and sediment transport equations need to be developed and verified to determine flow forces and subsequent erosion on embankments. Equations should adequately account for steep flow, shallow flow, and large bed form roughness relative to flow depth. For rock-protected embankments, the effects of large-scale roughness, element shape, and distribution need to be included. The equations should include the effects the rapidly accelerating part of overtopping flow.

2. Uniform flow equations do not apply to steep shallow flow or rapidly accelerating flow. Thus, for overtopping flow, friction factors need to be determined from hydraulic measurements and more comprehensive equations as noted in conclusion 1. For shallow flow, with relatively large-scale roughness elements, friction factors are a function of:

- Froude number F,
- shear velocity-element size Reynolds number U_*d/v,
- a projected drag area to flow area ratio, and
- a concentration function, λ, of roughness element spacing and distribution.

3. The separation of the energy slope, S, into the fractional part caused by form drag losses and the part caused by surface drag has been applied with some success in the bed form flow mechanics. This approach allows the similar separation of all hydraulic parameters such as flow velocity V, hydraulic radius R_h, tractive shear on the flow boundary, τ, and shear velocity U_*. This approach may help in handling large element roughness.

4. Because overtopping flow makes transition from plane shear flow to chute and pool flow, the steep flow friction factor, f, will vary with time as scour progresses. Different flow equations may be required during various phases of transition. To modify equations for handling chute and pool flow, will be difficult if at all possible.

5. For overtopping flow, model scaling sediment requires verified sediment transport equations that account for soil types ranging from noncohesive to fully cohesive. Based on existing uniform flow equations, it is expected that fully cohesive soil transport can be scaled according to model length ratio and noncohesive transport according to length ratio to the 3/2 power. A transition scaling function likely exists between the fully cohesive to noncohesive transport of soils.

6. For a highly transient event such as a breaching dam failure, model to prototype adjustment and verification is impossible. The difficulties are that model volumes and scour times are small.

7. Developing satisfactory equations for sediment transport in steep and very rough chute, and pool type flow may or may not be possible but will require much research. The development of reliable design methods may actually require full scale laboratory and prototype field testing. Much long-term effort is needed to develop adequate governing equations for rate of sediment transport over steep slopes. In reality, equations are needed not only for sediment, time, velocity scaling, and for mathematical modeling, but needed for more rational inferences from one prototype experience to another and to new design cases.

8. Random aspects related to overtopping flow such as the many variables, lack of true soil homogeneity, different soil classifications, and hydrograph variations present a strong case for more repetition of model tests and uniform documentation of failures in the field.

9. A well-coordinated interagency team approach is necessary to fund and make positive progress in solving a problem of this magnitude and expense.

10. The study of erosion during overtopping flow is a multivariable and multidisciplinary problem.

TECHNICAL CONSIDERATIONS AND ANALYSES

General Scour Considerations

Scour is a complicated interplay between soil properties, soil conditions, bed form, and flow characteristics. Furthermore, this interaction is complicated

2

by the loose interface between the flowing water and the sediment bed. Flow can change bed form due to scour, dune movement, and deposits. A change in bed shape, in turn, changes flow characteristics. Moving large particles can abrade an embankment. When these larger particles are not moving, they can cause local scour in their lee.

Soils have different grain size, d, distributions which help identify soil types. Fine-grained soil identification is complicated further by variations of cohesiveness that can be partially expressed by the PI (plasticity index) and the LL (liquid limit). It is desirable, but difficult, to express erosion resistance and transport in terms of soil properties, state of consolidation, construction methods, aging, and weathering. Ions in soil pores and flowing water can reduce or increase electrochemical surface activity bonding that produces cohesiveness.

Fluid shear, lift, drag, secondary flow, and turbulence are considered the main hydraulic factors affecting sediment transport. These factors vary with channel geometry, relative roughness, and Reynolds number.

Turbulence

A certain turbulent intensity may initiate movement. Once sediment is suspended, a somewhat less intense turbulence will keep particles in suspension. Turbulent intensity, ε_t , is the root mean square of the velocity fluctuations divided by the mean velocity; i.e..

$$\varepsilon_t = \frac{[(\overline{V'})^2]^{1/2}}{V}$$

where V' is velocity fluctuation about V the mean velocity.

Values of ε_t have been measured from 0.03 to 0.07. However, 0.1 is considered the value at which the velocity fluctuation can no longer be considered part of the main flow. Steep flow transition from plane shear flow to chute and pool flow is most likely related to this turbulent intensity near the 0.1 value. Turbulence at any point is strongly affected by flow section geometry, bed form, friction factor, f, fluid properties, location with respect to boundary and form disturbances just upstream.

Uniform Flow Equations for Tractive Shear Caused by Flow

For flow in canals and rivers, the simplest expression for average tractive shear, τ, can be determined from a free body diagram for normal flow.

$$\tau = \gamma R_h S \qquad (1)$$

where:
τ = average tractive shear on the flow boundary
R_h = hydraulic radius = A/P
A = flow section area
P = flow section wetted perimeter
S = slope of bed for normal flow or energy gradient for gradually varied flow having short reaches
γ = specific weight of water = density ρ times gravity g

Friction head loss for open channel flow can be expressed by the Darcy-Weisbach relationship as h_f:

$$h_f = f \left(\frac{L}{4R_h}\right) \frac{V^2}{2g} \qquad (2)$$

where:
h_f = friction loss in water head
f = Darcy-Weisbach friction factor $= \Phi\left(\frac{4R_h V}{v}, \frac{k_s}{4R_h}\right)$
L = reach length
R_h = hydraulic radius
V = average flow velocity
g = gravitational constant (acceleration)
v = kinematic viscosity
k_s = rugosity, boundary surface roughness

Slope is the same as h_f/L and specific weight, γ, equals density, ρ, times gravity g. Thus, equations (1) and (2) combine:

$$\tau = \frac{f\gamma V^2}{8g} = f\rho V^2/8 \qquad (3)$$

This equation clearly shows the relationship of tractive shear and the Darcy-Weisbach friction factor and velocity. For turbulent flow, the interrelationship between Darcy-Weisbach friction factor, f; Chezy coefficient, C; and Manning's, n, is:

$$\frac{1}{\sqrt{f}} = \frac{C}{\sqrt{8g}} = \frac{1.49 R_h^{1/6}}{n \sqrt{8g}} \qquad (4)$$

Various investigators [3 and 4] and others, have related tractive shear to vertical velocity profiles by logarithmic relationships. These equations can be reduced to two-point relationships. One example is the following:

$$\tau = \frac{(v_2 - v_1)^2}{2.5 \log_e (y_2/y_1)} \qquad (5)$$

The two velocities should be measured close to the bed or for relatively small values of distance, Y, from the bed not so close to the boundary that the pitot tube or other measuring devices are affected by boundary proximity.

3

Smeardon and Beasley [3] derived an equation for tractive shear for gradually varied flow using the definition on figure 1. The resulting equations for both velocity and unit discharge, q, are:

$$\tau = \gamma D \left[-\frac{VdV}{gdX} - \frac{dD}{dX} + \frac{dZ}{dX} \right] \qquad (6)$$

$$\tau = \gamma D \left[(q^2/gD^3 - 1)\frac{dD}{dX} + \frac{dZ}{dX} \right] \qquad (7)$$

For accelerating flow (dD/dX) is negative; for deceleration it is positive. Comparison of these with equation (1) shows the complications caused by gradually varying flow. Note that equations (6) and (7) reduce to equation (1) for uniform flow and small slopes.

A momentum approach was used to provide more insight into the nature of this type of flow because of the steepness and high acceleration of over-topping flow. Using the definition on figure 2—where φ is the slope angle between the bed and horizontal—the resulting equations for the velocity and unit discharge are:

$$\tau = \gamma D \left[-\frac{VdV}{gdX} - \cos\varphi \frac{dD}{dX} + \frac{\overline{D}}{D} \sin\varphi \right] \qquad (8)$$

$$\tau = \gamma D \left[\left(\frac{q^2}{gD^3} - \cos\varphi \right) \frac{dD}{dX} + \frac{\overline{D}}{D} \sin\varphi \right] \qquad (9)$$

For uniform flow and small slope, equations 8 and 9 also reduce to equation (1). Equations 8 and 9 govern design hydraulics and model flow over embankments and define, τ, for steep accelerating flow. Thus, equations such as (1) through (7) should not be used to input threshold tractive shear, τ_t, values for computing any of the other variables using the steep flow equations. Steep flow friction factor, f_s, and τ_t are strictly dependent variables best determined by measurements with steep flow and using steep flow equations (8) or (9). For steep fully developed smooth nonaccelerating flow, equation (1) can be used by using $\sin\varphi$ for the slope, S.

Limits of Uniform Flow Equation

Stable channel design and riprap design methods generally use uniform flow equations to obtain a design velocity or shear value and then use some form of particle entrainment function or critical velocity or shear value versus diameter. However, the uniform flow equations and friction factor function curves should not be used for relative roughness for $k_s/4R_h$ greater than 0.1 where R_h is the hydraulic radius and k_s is rugosity. Kamphius [5], and Brown and Chu [6] show that k_s is about two times d_{90}, where d_{90} is the size of the bed of which 90 percent of grains are finer. Since overtopping flow is highly accelerating and rapidly becomes shallow, the $k_s/4R_h$ limit needs to be carefully considered for design and modeling.
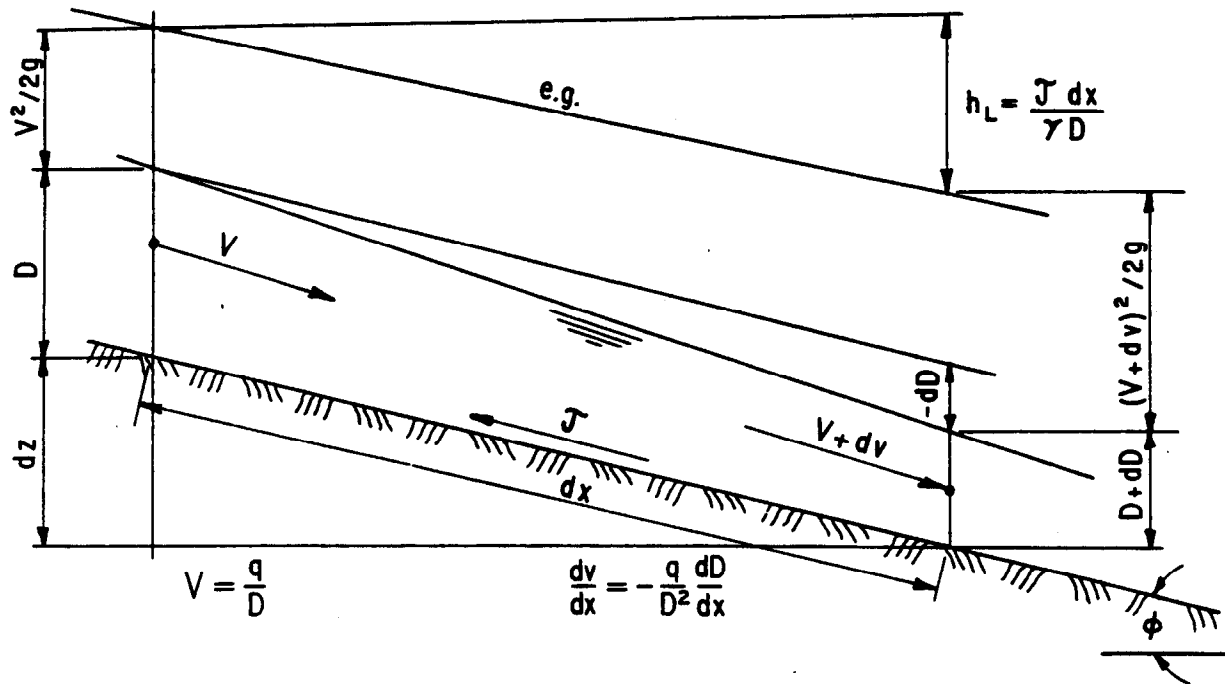

Figure 1. – Definition for gradually accelerating flow.
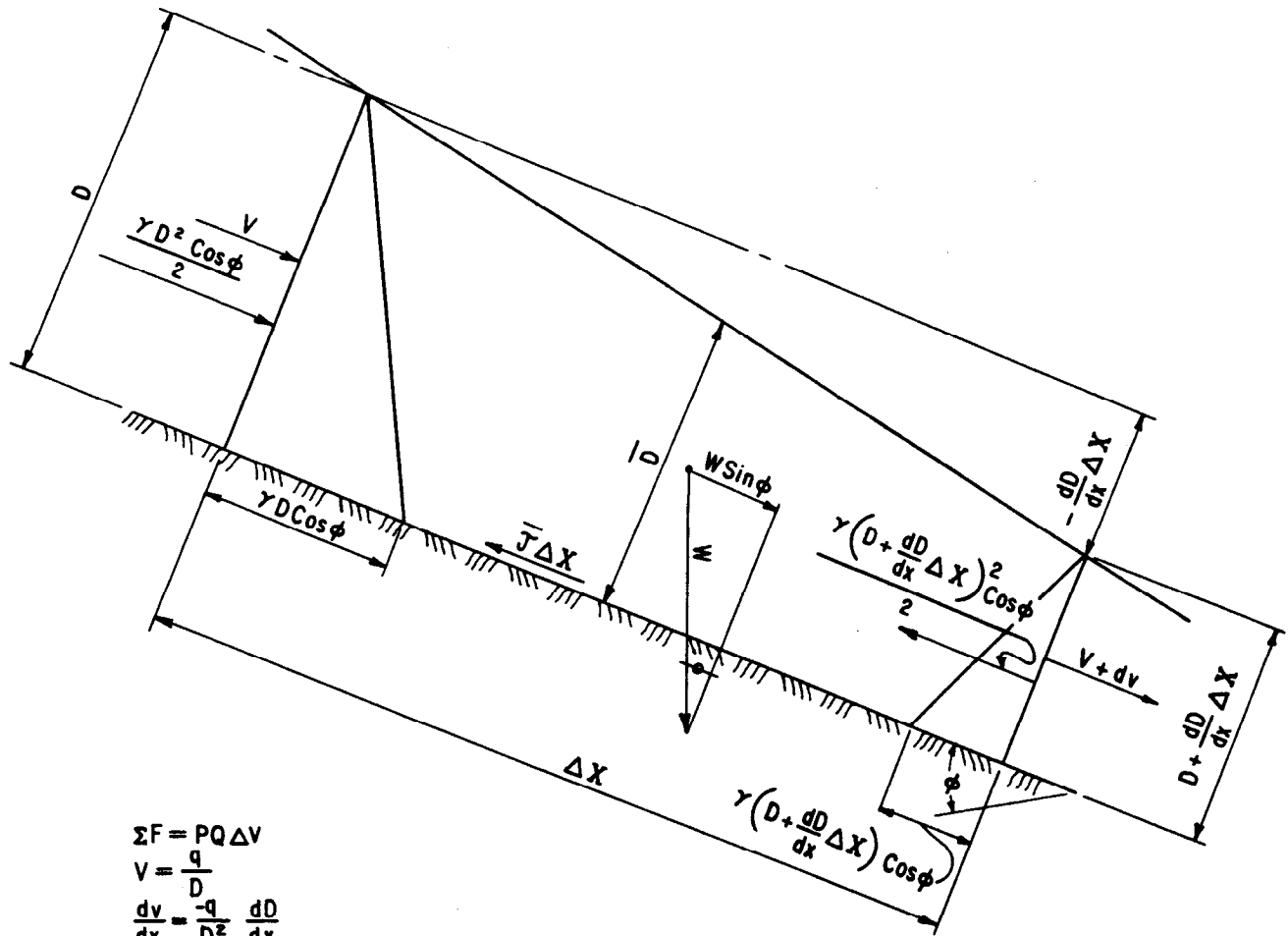
Figure 2. — Definition for momentum analysis.

$$\Sigma F = PQ \Delta V$$

$$V = \frac{q}{D}$$

$$\frac{dv}{dx} = \frac{-q}{D^2} \frac{dD}{dx}$$

Large Scale Roughness

Uniform flow friction loss equations have been used for rough, steep mountain flow. Also, some efforts have been made to extend friction loss concept to large-scale roughness distribution and element shape characteristics. Although these approaches still use equations such as equation (2), the steep flow friction factor, f_s, is no longer a simple function of Reynolds number and relative roughness. When relative roughness is greater than 0.1, roughness elements produce disturbances that reach the free surface causing gravity waves. Thus, shape and position distribution of the roughness elements become important. All equations and functions presented so far are limited by this maximum relative roughness value.

For example, Bathurst, Li, and Simons [7] propose the following relationship:

$$\frac{8}{f_s} = \Phi(R_{eg}) \times \Phi(F) \times \Phi(\lambda) \times \Phi\left(\frac{A_w}{WD}\right) = \frac{V^2}{gR_hS} \quad (10)$$

where:

f_s = steep flow and large element roughness friction factor
Φ = function operator
R_{eg} = a velocity-element size Reynolds number
F = Froude number
λ = roughness concentration parameter, a function of spacing, distribution of roughness elements, and element size relative to depth
A_w = wetted area that forces flow between roughness elements
W = width of rough element flow section
D = depth of flow section to the roughness datum
V = average flow velocity
g = gravitational constant (acceleration)
R_h = hydraulic radius, A/P
S = slope, horizontal to vertical

Friction values, f_s, determined by using functional relationships such as (10), if fully defined, could be used in uniform equations such as equations (2) and (3) to

5

calculate τ values in equations (8) and (9). The opposite is true in that τ values from equations (8) and (9) can be used in equations (2) and (3) to determine f_s values, that can be used to determine functional relationship (10) to define steep flow after flow acceleration has been completed.

Secondary Flow

When flow approaching a dam is deflected upward and accelerates, relatively mild secondary flow and bank eddies are stretched out horizontally and intensify into strong vortices. The reservoir approach flow has a strong influence on the strength and location of these vortices. Friction resistance and the reservoir approach side and bottom geometry govern the approach secondary flow and eddies that are intensified by upward deflection. Vortices are strong sediment carriers. In fact, vortex action is often deliberately produced to increase sediment sluicing efficiency at diversion dams. Side entrance contractions on the crest also cause vortex intensification. Thus, there are generally stronger vortices at each side of the crest with intermediate vortices across the remaining crest.

Even in symmetrical prismatic flow without upward deflected flow, secondary cell flow patterns develop. Knight and Patel [8] studied the structure of secondary flow in rectangular sections in terms of aspect ratio. Secondary flow cells will distribute along the boundary surface each with opposite rotation relative to its immediate neighbor. These investigators found that there is a step function, shown on figure 3, of aspect ratio versus the number of cells in one-half the flow section. Between opposing cell pairs, where circulation is downward, there is increased shear on the flow boundary. When flow conditions are such that depth to width ratios are near the rising parts of the curve, additional pairs of cells can attempt to form or temporarily make additional pairs and then break up. This type action can cause increased scour.

Crest Hydraulics and Crest Length

Flow over the crest of an embankment dam is similar to flow over a broad-crested weir having a sloping approach. Bos [9] summarizes flow regimes in terms of H/L for a rectangular weir profile, where H is total reservoir head above the crest and L is crest length (reach) in direction of flow. Understanding these regimes is required for insight into crest hydraulics. When

$$H/L < 0.08 , \qquad (11)$$

flow is subcritical over about 0.9 of the crest length (King [10]); friction of the crest controls and undulations can occur on the crest. These undulations
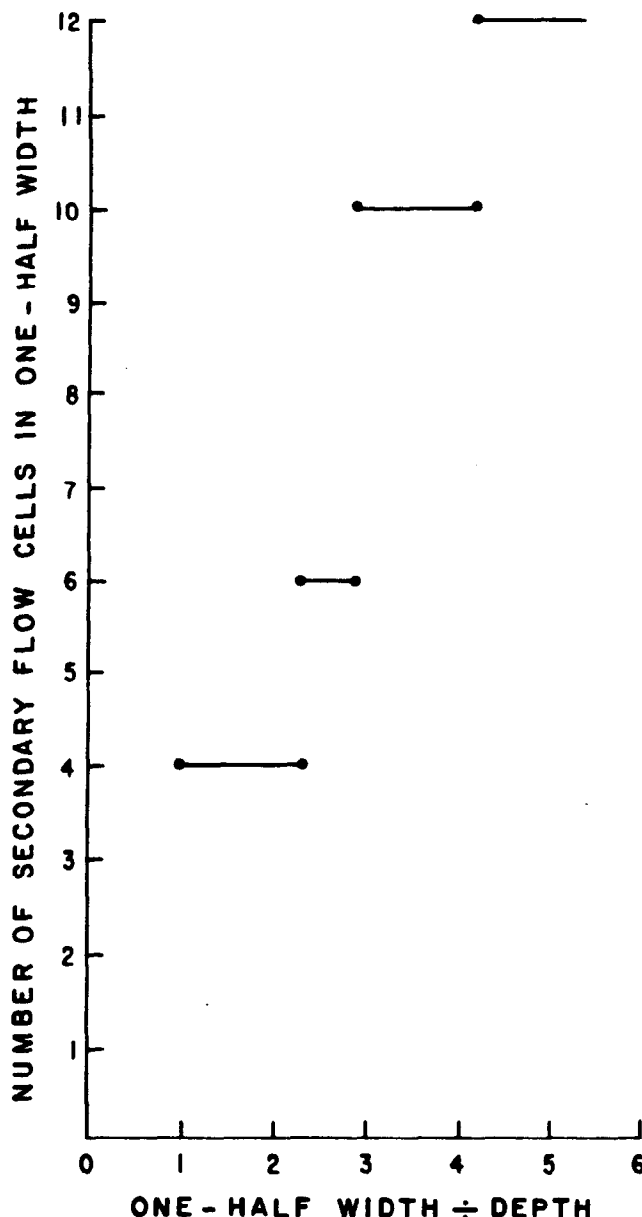
Figure 3. — Secondary flow cells in flow section, Knight and Patel [8].

could increase scour and decrease the time for development of chute and pool-type flow. When

$$0.08 < H/L < 0.33 , \qquad (12)$$

smoother parallel flow exists on more of the crest and the coefficient of discharge is constant in this range of H/L. Only while flow maintains inequality (12) does true smooth broad crested flow exist. When

$$0.33 < H/L < \text{from about 1.5 to 1.8} , \qquad (13)$$

parallel flow does not occur over the crest. Flow curvature causes increase in the coefficient of discharge,

6

and control is near the leading edge of the crest over a separation cavity. When

$$H/L > \text{about } 1.5 , \qquad (14)$$

flow becomes unstable and, depending on corner sharpness, can spring free. At H/L of 3 or greater, the flow acts like sharp-crested weir flow and is stable.

Basically, critical depth controls flow upstream on the crest. Relation for discharge Q at critical depth is:

$$Q = \left(\frac{gA_c^3}{a_c T_c}\right)^{1/2} \qquad (15)$$

If the limits of equation (12) are maintained, the critical depth generally occurs somewhere in the downstream one-third to one-fourth of the crest for any shape channel.

where:
Q = discharge
A_c = flow area for the entire critical depth or control location which varies with discharge
g = gravitational constant (acceleration)
a_c = velocity distribution coefficient or kinetic energy correction factor $v_c^3 \Delta A_c / V_c^3 A_c$ at the control section
T_c = top width at the control section
v_c = velocity for an incremental flow area, ΔA_c
V_c = average velocity of the entire control section

Using the equation of continuity; i.e., $Q = VA$, squaring and dividing both sides by 2, equation (15) can be rearranged:

$$\frac{a_c V_c^2}{2g} = \frac{A_c}{2T_c} \qquad (16)$$

Then specific energy, H_c, at the critical location can be written as:

$$H_c = D_c + (A_c/2T_c) \qquad (17)$$

At an upstream or reservoir reference location, specific energy, H_1, can be expressed as:

$$H_1 = D_1 + a_1 \frac{V_1^2}{2g} \qquad (18)$$

For a significant friction loss, h_f, the energy balance relative to crest elevation is:

$$H_1 = H_c + h_f \qquad (19)$$

and from equations (16) and (17):

$$D_c = D_1 + a_1 V_1^2/2g - A_c/2T_c - h_f \qquad (20)$$

Equations (15) and (20) define the crest hydraulics on an embankment. Values of 1.00 for a_1 and a_c are probably adequate for design—with present knowledge. However, for water measurement and mathematical models, studies concerning the effects of crest end conditions and the effects of being near critical depth for the value of a need to be further researched and measured.

Boundary Roughness Changes

When a change from fixed bed to movable bed flow, or the reverse occurs, local scour is caused by slight boundary offsets and boundary layer roughness. As discussed by Schlicting [11], Jacobs [12] studied the development of vertical shear distribution after the change of roughness, for both the smooth to rough and rough to smooth cases. Jacobs study shows that for fully developed approach flow, the shear stress at the bed immediately takes the new value, which is equal to that for fully developed flow for the new roughness. After a change in roughness, turbulence has to change its scale to adjust—affecting scour considerably.

Early Threshold Tractive Shear and Velocity Concepts

To attain useful scour and transport criteria, soil properties must be related to flow properties. For cohesionless soils, it is generally accepted that the mass of the largest sediment grain transported is proportionally related to velocity, V, raised to the sixth power. This proportionality suggests the possibility of a threshold of movement velocity, V_t, that will just move a particle of diameter, d. If particles are assumed to be spheres with constant specific weight, then weight, W, is proportional to the third power of diameter. Combining these two proportionalities results in:

$$V_t \propto d^{1/2} \qquad (21)$$

Also, equation (3) combined with equation (20) suggests the possibility of a threshold tractive shear, τ_t, or shear that will just move a particle of diamter, d, and:

$$\tau_t \propto d \qquad (22)$$

Relationships such as equations (21) and (22) are frequently used with some success. These relationships are really oversimplifications in terms of soil properties, soil conditions, and hydraulic conditions.

Generally, it is accepted that cohesion plays the most important part in scour resistance of clay soils. Sometimes the effects of cohesion are expressed by assuming that they are defined by a single soil parameter such as grain size only. Sometimes more complicated approaches assume that cohesion, C_o,

is a function of different combinations of soil parameters such as:

d_{50} = mean grain size,
σ = standard deviation grain size,
K_d = skewness of grain size,
%C = percent clay,
S_{vs} = vane shear strength,

C_s = compressive strength,
PI = plasticity index,
LL = liquid limit,
e = voids ratio, and others.

Relative Scour Resistance in Terms of Soil Classification and Properties

Through experience, engineers develop concepts of relative resistance of soils against erosion in terms of soil classification. For example, Bureau of Reclamation soils engineers [13] have ranked the relative resistance of different soil types in table 1. This ranking is for canals where soils were taken from borrow areas and recompacted.

When soils have 50 percent of their grain particles smaller than 0.074 millimeter in diameter, then plastic properties can contribute to erosion resistance in varying degrees from just slightly adding to the effects of grain size to being the dominant source of resistance. Plastic soil properties can be expressed at least partially by the following Atterberg limits [from ASTM (American Society for Testing Materials)]:

Liquid Limit (LL)—The moisture content corresponding to the arbitrary limit between the liquid and plastic states of consistency of a soil.

Plasticity Index (PI)—Numerical difference between the liquid limit and the plastic limit.

Plastic Limit (PL)—The moisture content corresponding to an arbitrary limit between the plastic and the semisolid states of consistency of a soil.

Figure 4 taken from Gibbs [13] shows the relative erosion resistance of cohesive soils in terms of LL and PI. The "A-line"† separates the clays from the silts below. It should be remembered that the threshold tractive shear ranking in this chart applies to disturbed soils that were recompacted to 90 lb/ft³ (11.34 N/m³). The threshold tractive shear ranges of the laboratory and field data used to derive this value are given next to the shading key (fig. 4). The plot indicates that the highest cohesive soils occur in a zone around LL of 35 percent and a PI of 15 percent.

Smeardon and Beasly [3] did correlations of threshold tractive shear with each of different soil properties that included PI, dispersion ratio, percent clay, and

mean particle size. Of these variables, they selected the PI and dispersion ratio as more strongly correlated. However, mean particle size correlated about as well. This is probably the result of electrochemical surface activity being strongly related to particle size. Data for these correlations were obtained in a flume with one clay reformed for tests.

Carlson and Enger [14] did multiple correlation analyses of various combinations of soil properties versus threshold tractive shear values with reformed samples of clay. They found that plastic properties and densities are the most important soil properties that affect scour resistance.

Tables 2, 3, and 4 were taken from Lane [15] who summarized the work of early investigators concerning threshold velocity and tractive shear. These tables include a few data for cohesive soils.

- Table 2—Etchevery's data for alluvial and clay soils ranged from about 0.10 to 0.43 lb/ft² (4.8 to 20.6 Pa).
- Table 3—Fortier and Scobey's data for alluvial silts to stiff clays, ranged from about 0.05 to 0.25 lb/ft² (2.4 to 12 Pa) for clear water and 0.15 to 0.46 lb/ft³ (7.2 to 22 Pa) for water transporting colloidal silts.
- Table 4 data ranged from about 0.02 to 0.63 lb/ft² (1 to 30.2 Pa).

It should be noted that these ranges include values of threshold tractive shear much higher than those obtained by Gibbs, Carlson and Enger, and Smeardon and Beasly for recompacted samples.

Kelly and Gularte [16] developed a threshold tractive shear equation that accounted for salt ion effects upon the cohesive strength of soil and a standard base measurement of rupture shear force angle.

The Bureau did threshold tractive shear tests on bedded clay samples taken from downstream of the Grand Coulee Third Powerplant. Several modes of erosion such as flaking and chunking were noted. Threshold tractive shear values ranged from 0.06 to 0.27 lb/ft² (2.87 to 12.93 Pa). Most of the observed modes of erosion were related to segregation of grain sizes and weaker cohesion in thin layers. Some segregation often occurs during construction of embankments.

Kamphius [17] determined that threshold tractive shear values for cohesive soil vary with:

compressive strength,
vane shear strength,
plasticity index,
percent clay, and
consolidation pressure.

---

†*Earth Manual*, Bureau of Reclamation, 2d ed., reprint 1985.

8

Table 1. – Soil classification with relative erosion stability

Major divisions of soils	Typical names of soil groups	Group symbols	Erosion resistance[*]
Fine-grained soils[1]			
	Inorganic silt, micaceous or diatomaceous fine sandy of silty soils, elastic silts	MH	–
Silts and clays *LL greater than 50*	Inorganic clays of high plasticity, fat clays	CH	12
	Organic clays of medium to high plasticity	OH	–
	Inorganic silts and very fine sands, rock flour, silty or clayey fine sands with slight plasticity	ML	–
Silts and clays *LL less than 50*	Inorganic clays of low to medium plasticity, gravelly clays, sandy clays, silty clays, lean clays	CL	11
	Organic silts and organic silt-clays of low plasticity	OL	–
Coarse-grained soils[2] *Sands[3]*	Silty sands, poorly graded sand-silt mixtures	SM	10
Sands with fines (appreciable	Clayey sands, poorly graded sand-clay mixtures	SC	7
amount of fines)	Sand with clay binder	SW-SC	6
Clean sands (little or no fines)	Well graded sands, gravelly sands, little or no fines	SW	8
	Poorly graded sands, gravelly sands, little or no fines	SP	9
Gravels[4]			
Gravels with fines	Silty gravels, poorly graded gravel-sand-silt mixtures	GW	5
(appreciable amount	Clayey gravels, poorly graded gravel-sand-clay mixtures	GC	4
of fines)	Gravel with sand-clay binder	GW-GC	1
Clean gravels (little or no fines)	Well graded gravels, gravel-sand mixtures, little or no fines	GW	2
	Poorly graded gravels, gravel-sand mixtures, little or no fines	GP	3
Highly organic soils	Peat and other highly organic soils	PT	–

[1]More than one-half of material is smaller than No. 200 sieve size. (The U.S.A. Standard series No. 200 sieve size is about the smallest particle visible to the naked eye).
[2]More than one-half of material is larger than No. 200 sieve size.
[3]More than one-half of coarse fraction is smaller than No. 4 sieve size. (For visual classifications, the ¼-inch size may be used as equivalent to the No. 4 sieve size).
[4]More than one-half of coarse fraction is larger than No. 4 sieve size.
[*]Numbers indicate the order of increasing values for the physical property name.
 Numbers indicate relative suitability (1 = best).

Entrainment Functions

Simons and Senturk [18] showed by dimensional analysis that noncohesive material has an entrainment function expressed as:

$$\frac{\tau_t}{(\rho_s - \rho)\, gd} = \Phi\left(\frac{U_{*t}d}{v}, \frac{d}{R_{ht}}, \frac{\rho_s}{\rho}\right) \qquad (23)$$

where:
s, t, & w = subscripts for sediment, threshold and water

f_t = friction factor at threshold of sediment motion
d = sediment diameter
g = gravitational constant (acceleration)
R_{ht} = hydraulic radius at threshold of sediment motion
S_t = slope of energy gradient at threshold of sediment motion
V_t = velocity at threshold of sediment motion
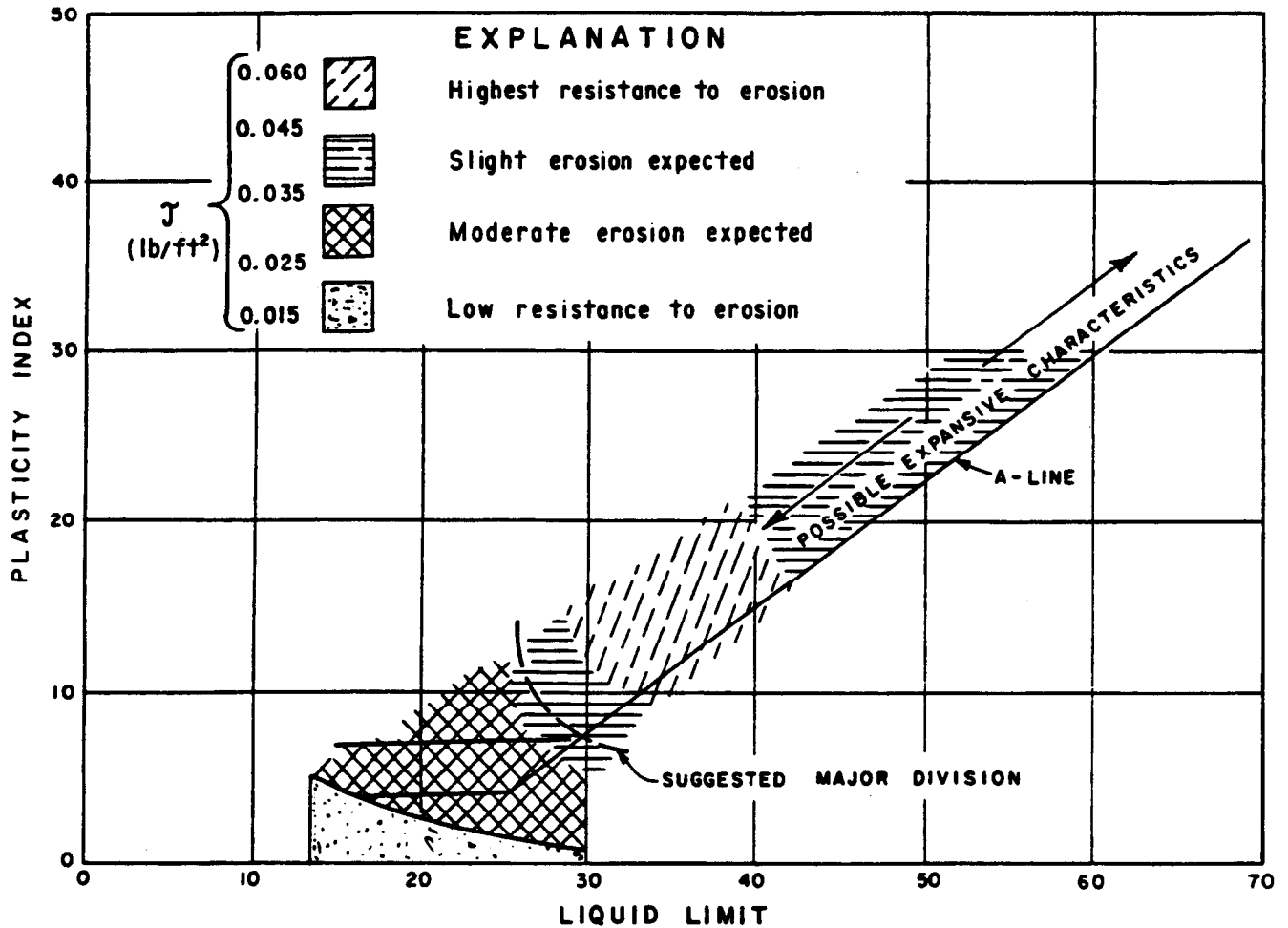τ_t = tractive shear at threshold of sediment motion

EXPLANATION

$$\mathcal{J}\ (lb/ft^2) \begin{cases} 0.060 \\ 0.045 \\ 0.035 \\ 0.025 \\ 0.015 \end{cases}$$

Highest resistance to erosion

Slight erosion expected

Moderate erosion expected

Low resistance to erosion

POSSIBLE EXPANSIVE CHARACTERISTICS

A-LINE

SUGGESTED MAJOR DIVISION

PLASTICITY INDEX

LIQUID LIMIT

Figure 4. – Erosion characteristics for fine-grained cohesive soils with respect to plasticity, Gibbs [13].

ρ = density of water
Φ = function operator
v = kinematic viscosity
U_{*t} = threshold shear velocity = $V_t \sqrt{f/8}$ = $\sqrt{gR_{ht}S_t} = \sqrt{\tau_t/\rho}$ and is a measure of turbulent intensity

This function has been defined empirically by Shields [19] after neglecting d/R_{ht} for relatively deep flow and ρ_s/ρ as relatively constant for sediment and water. Shields' entrainment function is shown on figure 5.

Using the pi term, d/R_{ht}, and valid pi term manipulation, d can be optionally replaced by R_{ht} in any of the other pi terms resulting in an equally valid but undefined relationship.

$$\frac{\tau_t}{(\rho_s - \rho) g R_{ht}} = \Phi\left(\frac{U_{*t}R_{ht}}{v}, \frac{d}{R_{ht}}, \frac{\rho_s}{\rho}\right) \qquad (24)$$

This manipulation reduces the use of d which is cumbersome to determine for clays and increases the use of hydraulic radius which is easier to establish.

The pi term, $\tau_t/[R_{ht}(\rho_s - \rho)g]$, is considered a dimensionless shear or a shear velocity Froude number squared and the term, $U_{*t}R_{ht}/v$, is the shear velocity flow section Reynolds number.

For clay, dimensionless cohesion, C_o; and density or compaction, P_c; parameters must be included. Again dropping the last two pi terms because of relatively deep flow, or relatively fine sediment, and for water and constant γ_s:

$$\frac{\tau_t}{(\rho_s - \rho) g R_{ht}} = \Phi\left(\frac{U_{*t}R_{ht}}{v}, C_o, P_c\right) \qquad (25)$$

This equation shows that threshold shear, τ_t, determined from a test device should be used for design with caution and an adjustment really needs to be made to account for lack of complete hydraulic similitude between the test device and actual flow. Krishnamurthy [20] gave an example with a comparison of threshold tractive shear values obtained for clays by a jet and a shear flume flow device. The threshold values were from 10 to 50 times greater

10

Table 2. – Comparison of Etchevery's maximum allowable velocities and tractive forces—from Lane [15].

Material	Manning's value used, n	Velocity ft/s	Tractive force lb/ft³
Very light pure sand of quicksand character	0.020	0.75 to 1.00	0.006 to 0.001
Very light loose sand	.020	1.00 to 1.50	.011 to .025
Coarse sand or light sandy soil	.020	1.50 to 2.00	.025 to .045
Average sandy soil	.020	2.00 to 2.50	.045 to .070
Sandy loam	.020	2.50 to 2.75	.070 to .084
Average loam, alluvial soil, volcanic ash soil	.020	2.75 to 3.00	.084 to .100
Firm loam, clay loam	.020	3.00 to 3.75	.100 to .157
Stiff clay soil, ordinary gravel soil	.025	4.00 to 5.00	.278 to .434
Coarse gravel, cobbles, and shingles	.030	5.00 to 6.00	.627 to .903
Conglomerate, cemented gravel, soft slate, tough hardpan, soft sedimentary rock	.025	6.00 to 8.00	.627 to 1.114

1 ft/s = 0.3048 m/s, and 1 lb/ft² = 47.88 Pa.

for the jet device relative to those obtained with shear flow device. Thus, if the function in equation (25) was defined, it might help to evaluate test facilities and to account for scale effects between erosion test facilities, models and flow channels with cohesive beds.

Gravity Effects on Erosion Resistance

Because riprap and gravel blankets could possibly be used to protect embankments, slope-gravity effects were considered. The assumptions of Carlson [21] were used. The main hypothesis used was that resistance to motion on a side slope and on the flat bottom is equal to the normal force times the tangent of the angle of repose, θ, of the bed material. Angle of repose, θ, is the angle between the horizontal and the maximum slope that a soil assumes through natural processes. For dry granular soils, the effect of the height of slope is negligible; for cohesive soils, the effect of height of slope is so great that the angle of repose is meaningless (ASTM). Brooks [22] expanded the relationship for flow on the slope in any direction resulting in:

$$\frac{\tau_s}{\tau_l} = \frac{\sin\varphi \sin\beta}{\tan\theta} + \sqrt{\left(\frac{\sin\varphi \sin\beta}{\tan\theta}\right)^2 + \cos^2\varphi \left[1 - \left(\frac{\tan\varphi}{\tan\theta}\right)^2\right]} \quad (26)$$

When β is 0 or when flow parallels the canal side slope in the direction of the channel axis, the equation simplifies to Carlson's previous relationship.

$$\frac{\tau_s}{\tau_l} = \cos\theta \left(1 - \frac{\tan^2\varphi}{\tan^2\theta}\right)^{1/2} = \sqrt{1 - \left(\frac{\sin\varphi}{\sin\theta}\right)^2} \quad (27)$$

where:

τ_s = threshold tractive shear for a sediment particle on a slope

τ_l = threshold tractive shear for same particle on a level bottom

θ = angle of repose for noncohesive material

β = angle of flow relative to a horizontal line in the plane of the embankment face

φ = slope, angle of canal or dam embankment

s & l = subscripts for a sloped bed and a level bed

For this study, an analysis was made for uphill and downhill flow resulting in:

$$\frac{\tau_s}{\tau_l} = \frac{\sin(\theta \pm \varphi)}{\sin\theta} \quad (28)$$

It can be shown that Brooks' general equation (26) reduces to equation (28) for β of 90 and 270 degrees. This function is plotted for both the uphill and downhill case on figure 6.

Angle of repose, θ, varies from 27 to 42 degrees. Figure 7, taken from Simons [23], shows that angle of repose varies with size and angularity of particle. For convenience in riprap design, threshold tractive shear can be related to velocity using equation (3) which results in:

$$\tau_s/\tau_l = V_s^2/V_l^2 \quad (29)$$

Equation (26) is derived by setting the ratio of resultant forces tending to cause motion to the forces resisting motion equal to the tangent of internal shear resistance angle. For noncohesive soils in loose state, angle of repose, θ, is nearly equal to the shear resistance angle just at rupture. Figure 6 indicates that noncohesive material with angle of repose at 34 degrees on 6:1 downhill slope has about 75 percent of the critical tractive shear resistance of that for the same material on a flat bed. As this slope increases, erosion resistance decreases rapidly; as slope decreases, erosion resistance increases slowly. Noncohesive material on a 4:1 slope has about 60 percent erosion resistance relative to flat bed flow resistance. For cohesive soil, equations (27) through (29) need to be modified by incorporating Coulomb's equation for shear resistance at rupture.

Sediment Transport Functions

Shields' entrainment function, figure 5, can be considered a transport function for a special case where

Table 3. – Comparison of Fortier and Scobey's limiting velocities and tractive force values—from Lane [15].

Material	n	For clear water		Water transporting colloidal silts	
		Velocity ft/s	Tractice force lb/ft²	Velocity ft/s	Tractive force lb/ft²
Fine sand colloidal	0.020	1.50	0.027	2.50	0.075
Sandy loam noncolloidal	.020	1.75	.037	2.50	.075
Silt loam noncolloidal	.020	2.00	.048	3.00	.11
Alluvial silts noncolloidal	.020	2.00	.048	3.50	.15
Ordinary firm loam	.020	2.50	.075	3.50	.15
Volcanic ash	.020	2.50	.075	3.50	.15
Stiff clay very colloidal	.025	3.75	.26	5.00	.46
Alluvial silts colloidal	.025	3.75	.26	5.00	.46
Shales and hardpans	.025	6.00	.67	6.00	.67
Fine gravel	.020	2.50	.075	5.00	.32
Graded loam to cobbles when noncolloidal	.030	3.75	.38	5.00	.66
Graded silts to cobbles when colloidal	.030	4.00	.43	5.50	.80
Coarse gravel noncolloidal	.025	4.00	.30	6.00	.67
Cobbles and shingles	.035	5.00	.91	5.50	1.10

1 ft/s = 0.3048 m/s, and 1 lb/ft² = 47.88 Pa.
n = Manning's n

Table 4. – U.S.S.R. limiting velocities and tractive forces in cohesive material—from Lane [15].

Descriptive term Voids ratio range	Compactness of sediment bed							
	Loose 2.0 to 1.2		Fairly compact 1.2 to 0.6		Very compact 0.6 to 0.3		Compact 0.3 to 0.2	
Principal cohesive material of bed	Limiting mean velocity ft/s and limiting tractive force lb/ft²							
	ft/s	lb/ft²	ft/s	lb/ft²	ft/s	lb/ft²	ft/s	lb/ft²
Sandy clays (sand content less than 50%)	: 1.48	0.040	2.95	0.157	4.26	0.327	5.90	0.630
Heavy clayey soils	: 1.31	.031	2.79	.141	4.10	.305	5.58	.563
Clays	: 1.15	.024	2.62	.124	3.94	.281	5.41	.530
Lean clayey soils	: 1.05	.020	2.30	.096	3.44	.214	4.43	.354

1 ft/s = 0.3048 m/s, and 1 lb/ft² = 47.88 Pa.

transport is nearly equal to zero. Gessler's [24] modification of Shields' function, figure 8, with parallel curves for different probabilities of moving, further indicates that transport is related to the Shields' parameters and approximately parallels Shields' critical curve. Graf and Pazis [25] make an even firmer connection to transport by developing nearly parallel curves, figure 9, to Shields' curve in the transition zone in terms of the number of particles moving. Thus, it seems quite logical that Shields' parameters should define higher and very active transport as well as incipient motion of sediment. For modeling, the most useful form for noncohesive sediment transport function is given by Taylor, figure 10, and discussed by Vanoni [26]. Taylor uses a dimensionless sediment discharge parameter as a third or nesting parameter along with Shields' parameters (fig. 5). The dimensionless sediment discharge parameter, q_{s*}, is defined as:

$$q_{s*} = q_s/U_*d \tag{30}$$

where:
q_s = sediment discharge in volume per unit width per second

U_* = shear velocity
d = diameter of sediment particle

Taylor curves of dimensionless discharge, q_{s*}, are approximately parallel to Shields' curve, including the transition dip, figure 10. The extension of this function for larger sediment discharge would be of considerable benefit to modelers. Thus, model sediment discharge scaling requires investigating the following functional relationship:

$$\frac{q_s}{U_*d} = q_{s*} = \Phi\left(\frac{\tau}{(\rho_s - \rho) gd}, \frac{U_*d}{\nu}\right) \tag{31}$$

Replacing d with R_h by pi term manipulation and adding dimensionless cohesion and compaction terms might be a good approach for investigating cohesive transport. Then the undefined but equally valid transport function can be written as:

$$\frac{q_s}{U_*R_h} = \Phi\left(\frac{\tau}{(\rho_s - \rho) g R_h}, \frac{U_*R_h}{\nu}, C_o, P_c\right) \tag{32}$$

12

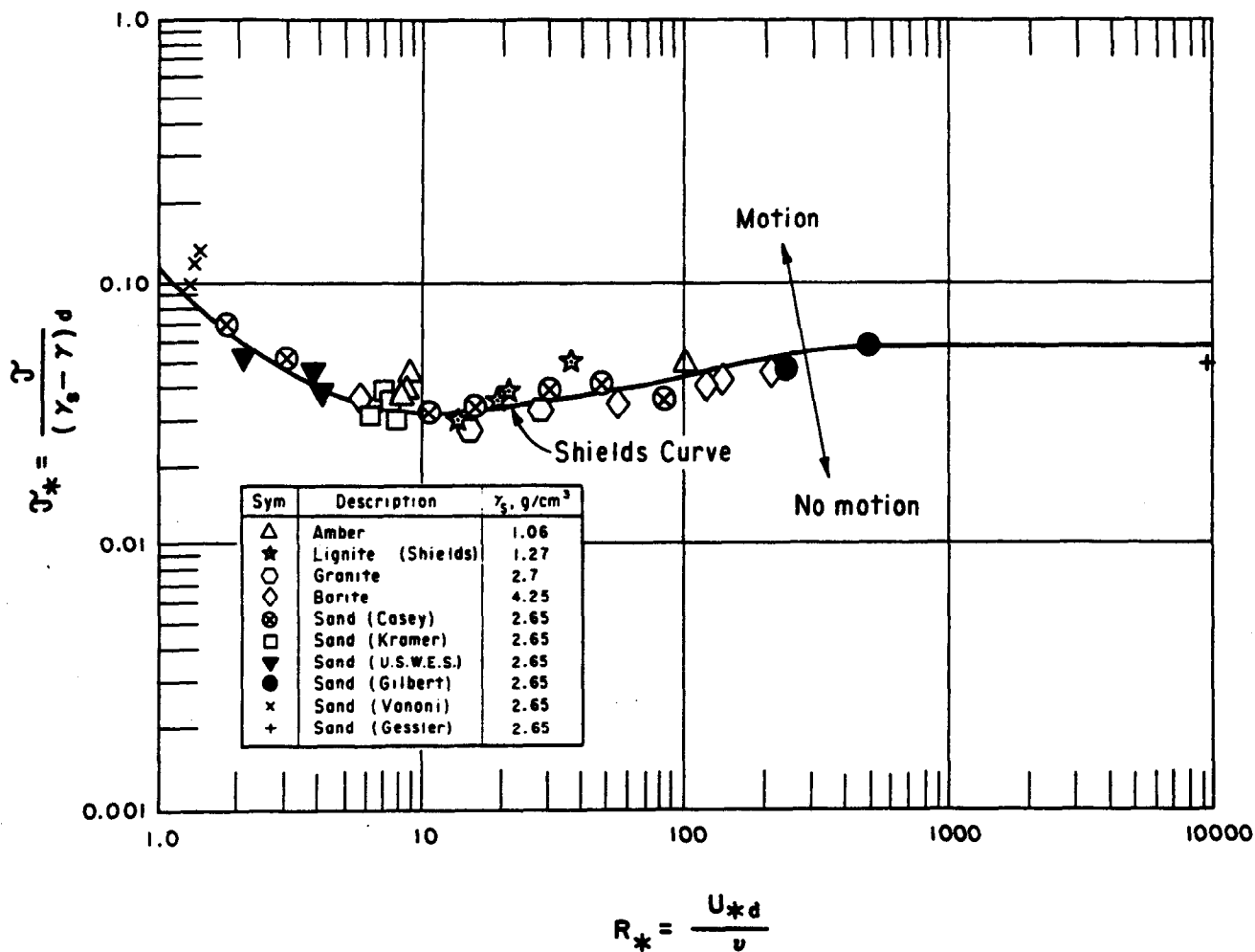| Sym	Description	γ_s, g/cm^3
△	Amber	1.06
☆	Lignite (Shields)	1.27
◯	Granite	2.7
◇	Barite	4.25
⊗	Sand (Casey)	2.65
□	Sand (Kramer)	2.65
▼	Sand (U.S.W.E.S.)	2.65
●	Sand (Gilbert)	2.65
×	Sand (Vanoni)	2.65
+	Sand (Gessler)	2.65

$$R_* = \frac{U_* d}{v}$$

Figure 5. — Shields [19] diagram for threshold of bed material movement.

13

V_{tl} = Velocity at threshold of sediment motion for flow over level bed
V_{ts} = Velocity at threshold of sediment motion for flow over sloped bed
Z = Horizontal component of bed slope
τ_{tl} = Tractive shear at threshold of sediment motion for flow over level bed
τ_{ts} = Tractive shear at threshold of sediment motion for flow over sloped bed
θ = Angle of repose for bank material
φ = Slope angle of embankment

$$\frac{\tau_{ts}}{\tau_{tl}} \propto \frac{V_{ts}^2}{V_{tl}^2}$$

Uphill →

$\dfrac{\tau_{ts}}{\tau_{tl}} = \dfrac{\sin(\theta + \varphi)}{\sin\theta}$

2.00

1.80

1.60

1.40

1.20

Z = 1.10
Z = 1.50
Z = 2.0
Z = 2.5
Z = 3.0
Z = 4.0
Z = 5.0
Z = 6.0
Z = 10.0
Z = 20.0

Z = 1.25

Flat 1.00

Z = 20.0
Z = 10.0
Z = 6.0
Z = 5.0
Z = 4.0
Z = 3.0
Z = 2.5
Z = 2.0

0.80

0.60

0.40

$\dfrac{\tau_{ts}}{\tau_{tl}} = \dfrac{\sin(\theta - \varphi)}{\sin\theta}$

← Downhill

0.20

Z = 1.50

0.00

Z = 1.25

26   28   30   32   34   36   38   40   42
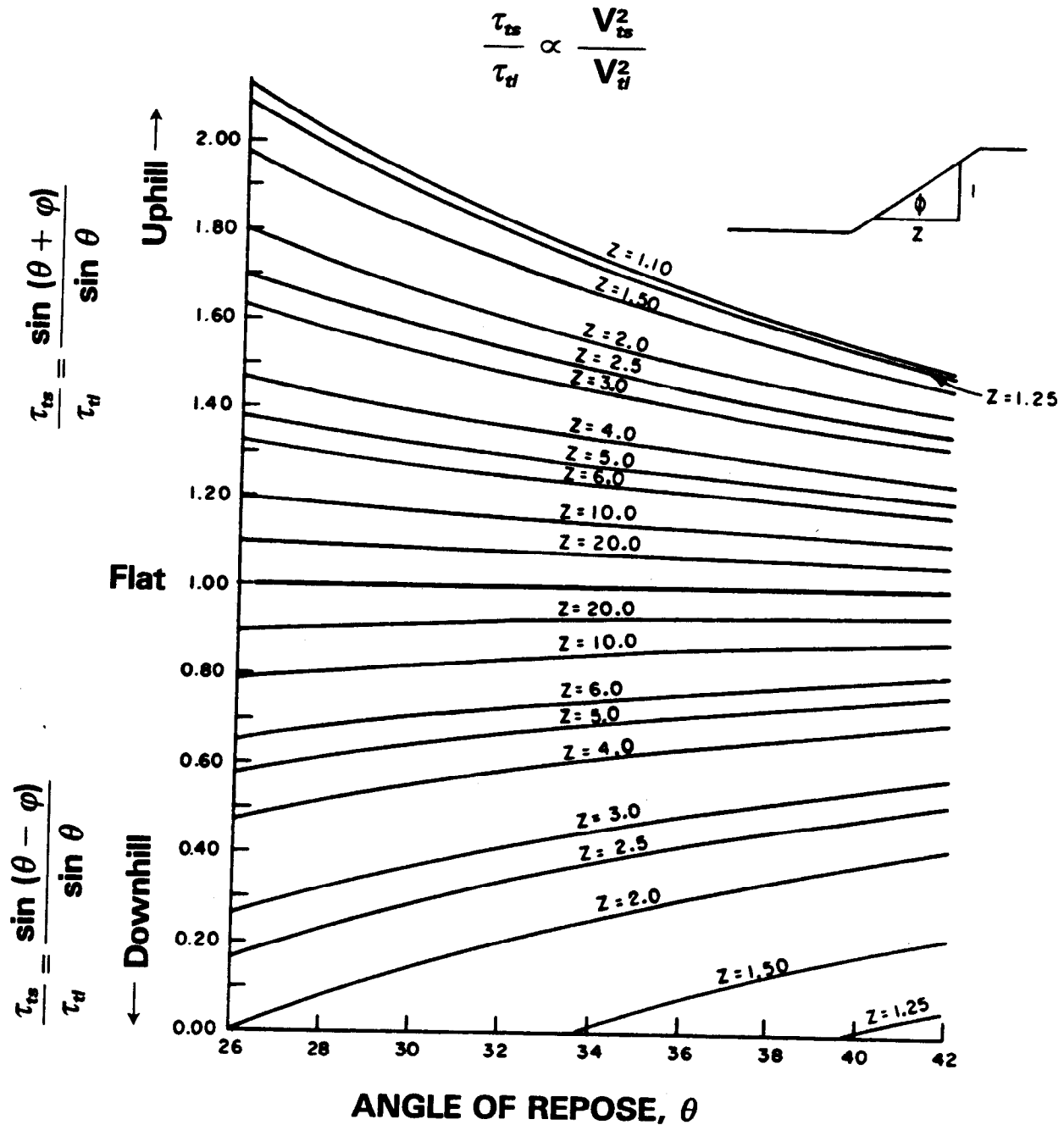
ANGLE OF REPOSE, θ

Figure 6. — Embankment stability correction factor for slope gravity effect during uphill and downhill flow.
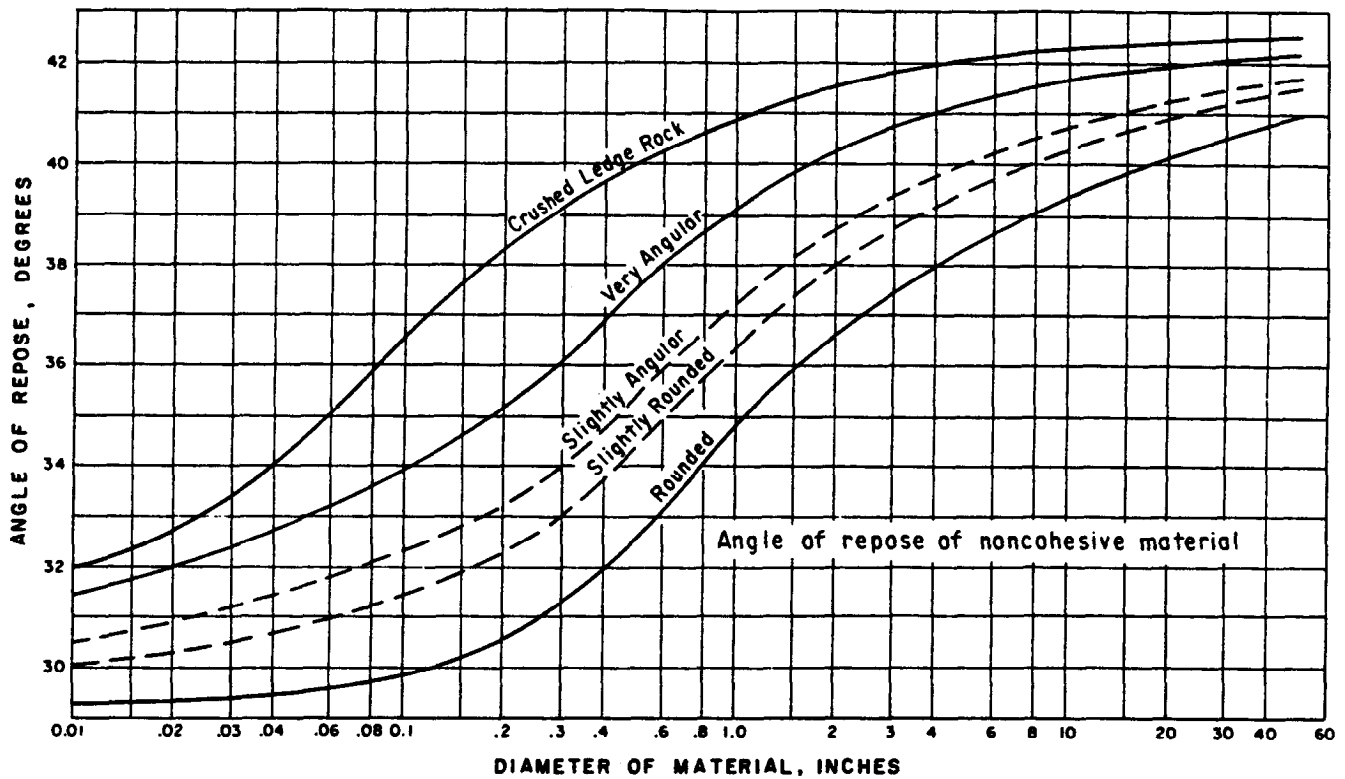
14

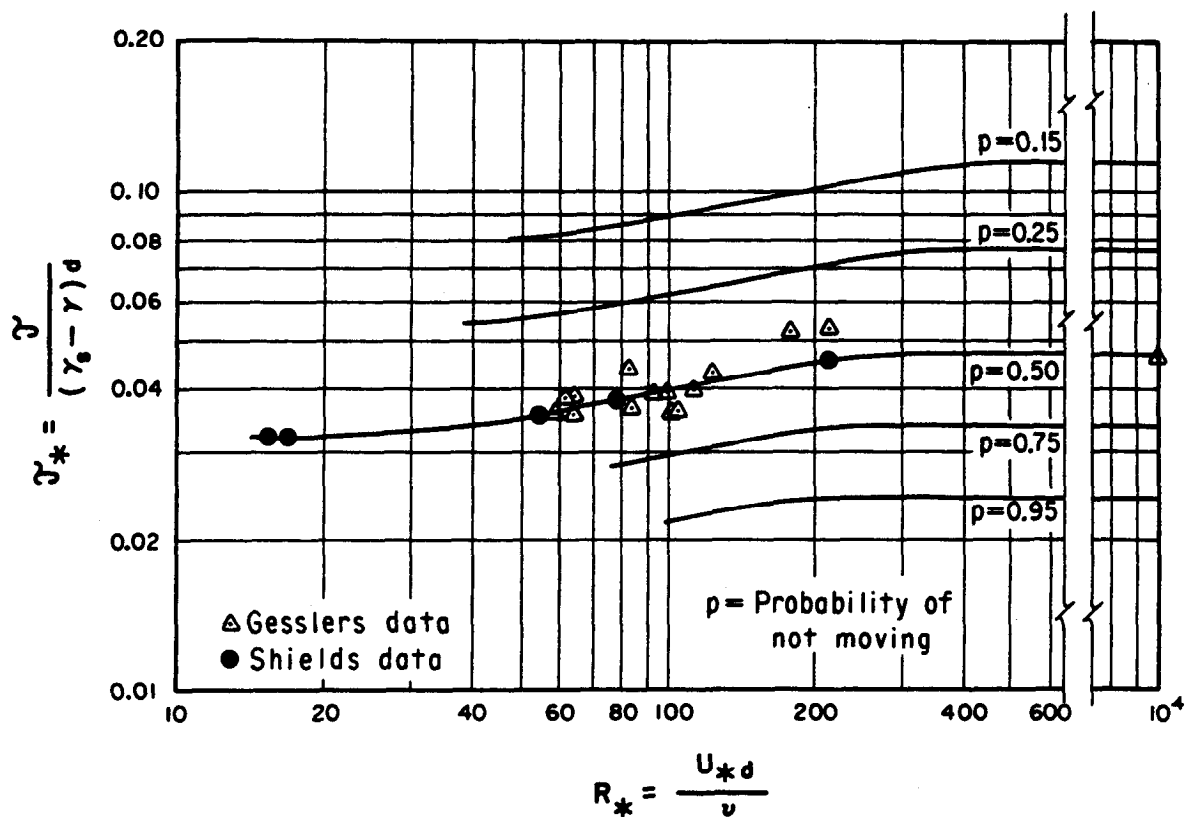Figure 7. – Angle of repose for rock materials, Simons [23].

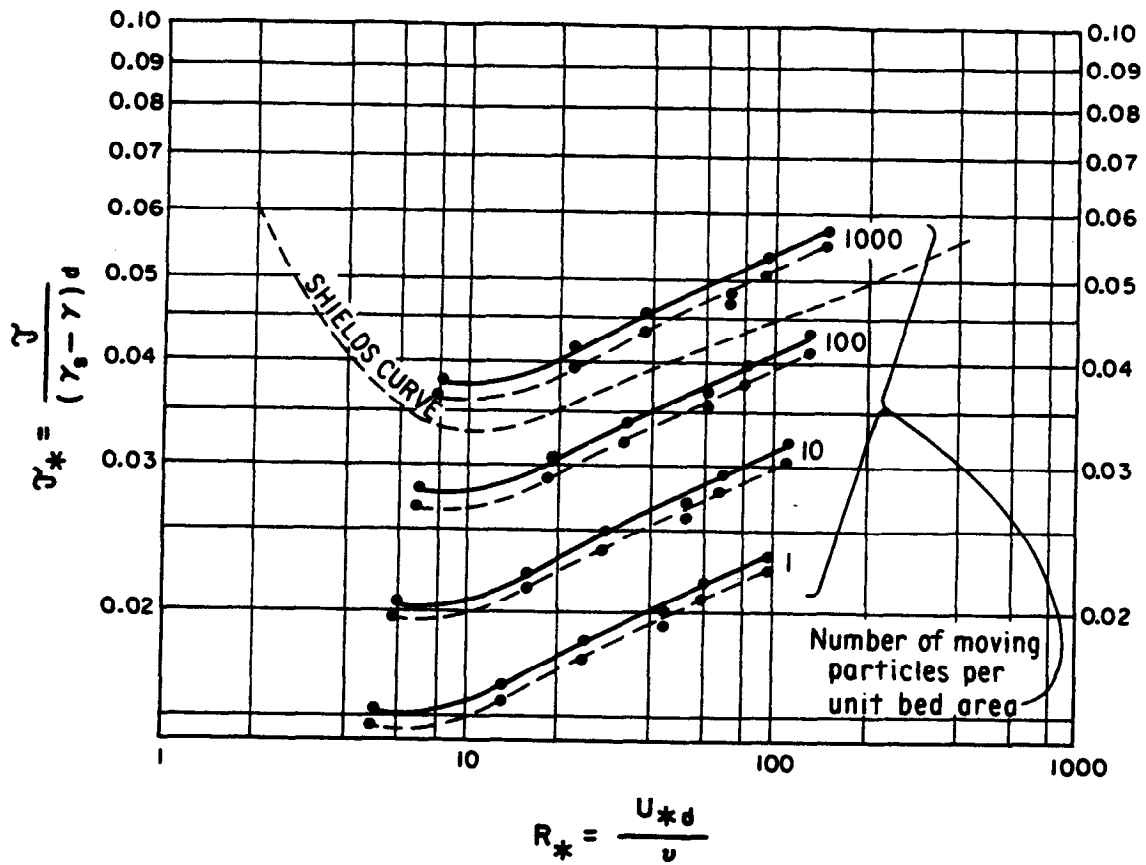Figure 8. – Gessler's [24] probability modification of Shields' [19] function.

15

Figure 9. — Graf and Pazis' [25] modification of Shields' [19] entrainment function. N'' is number of moving particles per unit bed area.
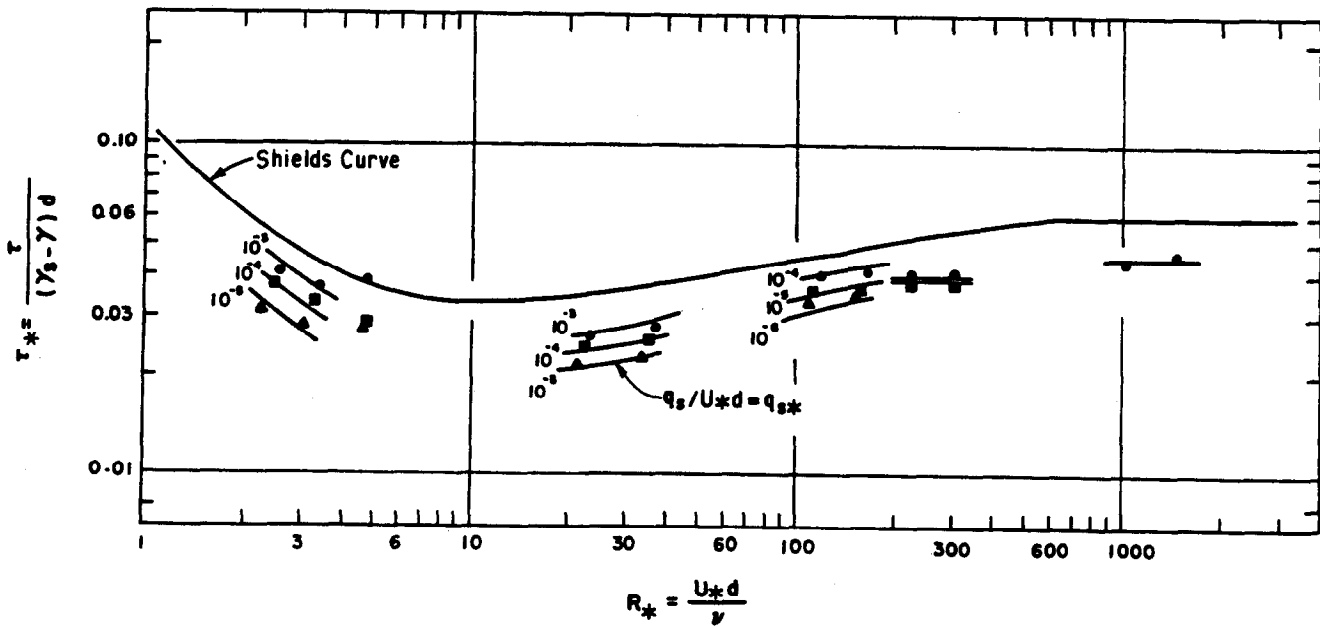

Figure 10. — Taylor's dimensionless sediment discharge plotted with Shields' function, Vanoni [26].

16

For shallow flow, relative roughness $(k_s/4R)$ would have to be added. Further adjustment in terms of the parameters such as in equation (10) also would be needed to account for large scale bed form roughness.

Metha et. al. [27] recommended Kandiah's [28] equation that indicates mass erosion rate varies linearly with excess shear $(\tau - \tau_c)$ and expressed erosion rate as:

$$q_m = \frac{k_m(\tau - \tau_t)}{\tau_t} \tag{33}$$

where:

q_m = mass of sediment per unit area per second
τ = tractive shear on the flow boundary
τ_t = threshold tractive shear
k_m = an erodibility constant

Chen [29] uses a volume form of excess shear equation developed by Ariathurai and Arulanadan [30] expressed as:

$$q_v = k_v(\tau - \tau_t)^n \tag{34}$$

where:

q_v = volumetric sediment discharge for unit area in $(ft^3/s)/ft^2$
k_v = 0.00005 for both cohesive and noncohesive soils
n = 1.0 for cohesive soil and 1.5 for noncohesive soil

General Model Similitude

To represent actual conditions, a model must be geometrically, kinematically, and dynamically similar to the prototype. If a model is not fully similar in any one or more of these three aspects, care must be taken to account for or minimize distortion. At times, models can be physically distorted in ways of less importance tending to compensate for the defect of other more important variables. Occasionally, with care, data from a defective model can be corrected by analysis or previous experience. However, if distortions are too large or too numerous, a model will not represent the prototype in any way and interpretations or data correction by analysis will be fruitless. These same similitude considerations also apply to combining results from different shear erosion test devices or to applying a threshold tractive shear value from any one test device to an actual river or channel case.

Hydraulic Friction and Flow Scaling

The most accurate and efficient modeling can be accomplished by using the similitude and approximation method of Klein [31] when governing equations are available and applicable to both the model and and prototype. For model analysis, the equations are put into dimensionless form by normalizing the variables by defining dimensionless variables using characteristic boundary values to replace dimensional variables. Characteristic or boundary values and physical constants are separated from the dimensionless variables into groups in each equation term. Dividing one of the groups into all the remaining groups results in dimensionless parameters or (pi) terms which are attached as coefficients to specific terms of the dimensionless equation. These pi terms can be evaluated for both the model and prototype. Thus, scaled effects of a model can be quantified provided the characteristic boundary values in the pi terms have been carefully selected.

For overtopping flow, using equation (8) and applying the similitude and approximation method of Kline [31] results in:

$$\frac{\tau_*}{D_*}\left(\frac{f}{8}\right)\frac{V_c^2}{gX_c} =$$

$$- V_*\frac{dV_*}{dX_*}\left(\frac{V_c^2}{gX_c}\right) - \cos\varphi\,\frac{dD_*}{dX_*} + \frac{\overline{D}_*}{D_*}\sin\varphi \tag{35}$$

where:

$\tau_* = 8\tau/f\rho V_c^2$
$V_* = V/V_c$
$X_* = X/X_c$
$\overline{D}_* = \overline{D}/X_c$
$D_* = D/X_c$
$dV_* = dV/V_c$
$dX_* = dX/X_c$
$dD_* = dD/X_c$
φ = flow channel slope angle
X_c = linear characteristic boundary value
V_c = characteristic boundary velocity value

Asterisks denote dimensionless variables, c denotes characteristic or bondary values. The term V_c^2/gX_c (the Froude number squared) and f (the Darcy-Weisbach friction factor) should be the same for both a model and its prototype. Satisfying this requirement would ensure that forces, turbulence, and secondary flows are similar between model and prototype.

Making the Froude number and friction factor the same for model and prototype is difficult to do and often cannot be achieved. However, effort should be made to determine by means of the dimensionless equation the degree and effects of any deficiency in the interpretation and use of data obtained with a model. By tradition, the model value for V_c^2/gX_c is made equal to the prototype for a free surface model making necessary use of analysis, field data, and best estimates to check friction, sediment entrainment, and transport scaling.

In equation (35) the pi term attached to shear term is a product blend of friction factor f and Froude number squared, F^2. For Froude scaling, the Froude number is set equal for both the model and prototype. Thus, f should be made the same for both the model and prototype. The friction factor, f, is a function of Reynolds number, $4R_hV/v$, and relative roughness, $k_s/4R_h$, and the modeler can check frictional scaling with Nikuradse-type friction curves.

Sediment Transport Rate Scaling

Settling velocity or fall velocity is closely related to the phenomena of sediment being entrained in the flow and how long it will travel once lifted off the bed into the flow. Settling velocity scales by Froude law when model sediment diameters are equal to or greater than 1.0 millimeter.

If equation (31) is accepted, then to scale noncohesive sediment discharge, the dimensionless sediment discharge parameter q_s/U_*d should be made the same for both model and prototype. On this basis, sediment discharge would scale as $L_r^{3/2}$. Bagnold [32] shows that rate of noncohesive sediment transport is proportional to τ to the 3/2 power times a soil erosion efficiency constant k. If the efficiency constant for model and prototype are equal, then by Froude law τ scales according to L_r, and sediment volume transport rate, q_s, scales as $L_r^{3/2}$.

If an excess tractive shear equation like (33) is accepted for cohesive soil and for dimensional units of k—same as for q_s, then

$$q_s = k \frac{\tau - \tau_t}{\tau_t} \qquad (36)$$

For field recompacted cohesive soils of canals τ_t is generally less than 0.07 lb/ft² (3.31 Pa). For geologically compacted clay τ_t is generally less than 0.40 lb/ft² (19.15 Pa). Tractive shear such as would occur for steep flow is large, greater than 15 lb/ft² (718 Pa). Thus, τ_t can be ignored in the numerator and

$$q_s = k \frac{\tau}{\tau_t} \qquad (37)$$

Using equation (3) and (37) results in

$$q_s = k\rho \left(\frac{f}{8}\right) \frac{V^2}{\tau_t} \qquad (38)$$

For a given soil, (τ_t) in the denominator in these equations can be incorporated with the soil erosion constant k and cohesive sediment discharge would scale as L_r, the length ratio. It is noted that V^2/τ_t is the same term that Abt [33] uses for the transport function.

In deriving equation (35) dimensionless shear τ_* was defined as:

$$\tau_* = 8\tau/\rho f V_c^2$$

Using equation (37), τ_* can be redefined as:

$$\tau_* = \frac{8}{f} \left(\frac{q_s}{k}\right) \frac{\tau_t}{\rho V_c^2} \qquad (39)$$

Substituting into equation (35) results in:

$$\frac{q_s}{k} \left(\frac{1}{D_*}\right) \left(\frac{V_c^2}{gX_c}\right) \frac{\tau_t}{\rho V_c^2} \qquad (40)$$

$$= -V_* \frac{dV_*}{dX_*} \left(\frac{V_c^2}{gX_c}\right)$$

$$- \cos\varphi \frac{dD_*}{dX_*} + \frac{\overline{D_*}}{D_*} \sin\varphi$$

Thus

$$\frac{q_s}{k} = \Phi \left(\frac{V_c^2}{gX_c}, \frac{1}{D_*}, \frac{\tau_t}{\rho V_c^2}, \varphi \right) \qquad (41)$$

In this equation, k has the same dimensions as q_s. Also, k, f, and τ_t must relate to modes of flow such as chutes and pool. In modeling, the Froude number squared V_c^2/gX_c is made the same for both the model and prototype. When a model scale L_r has been selected, Reynolds number is distorted making manipulation within functions such as equation (10) required to attain equal f for both model and prototype.

Based on equations (31) and (32) and complete similitude, embankment sediment discharge scales to $L_r^{3/2}$ for noncohesive soils possibly making transition toward a linear relationship with respect to L_r as soils become more cohesive. However, cohesive sediment discharge rate and scour time scaling are really contingent upon completely satisfying equation (40) or by making adequate scale adjustments by means of the equation for any model distortions deliberately or unintentionally incorporated in a model.

For ideal scaling, there also should be transient time similitude in terms of roughness and mode of flow changes during scour changes of bed shape.

LABORATORY MODEL STUDIES

Model Study Program

To help resolve scaling problems and for design considerations, it was decided that three typical embankment soils would be tested. Also, because of

known and possible limits of the transport equations (29), (33), and (36) it was originally decided to use three different unit discharges for tests. Later, however, tests were mainly directed toward supporting Bureau of Reclamation designers and the National Park Service in modifying two dams in Blue Ridge Parkway, North Carolina, to permit some overtopping without major erosion. Thus one type of soil was tested.

Model Scaling Used for Laboratory Test Runs

Scaling is limited by not having a fully verified cohesive transport equation. Equation (40) is fully valid on the right side. However, the left side is only as valid as equation (37) and the care in its use. The variation of f, possible variation of the erodibility constant, k, during erosion and changing modes of flow still preclude the use of equation (40) for exact scaling.

Without verified equations, fully reliable sediment transport time and velocity scaling relationships can not be determined. This is not only a problem in using a small model but is also a hindrance in making predictions from experience with one full-sized embankment to another full-sized embankment. To estimate sediment transport scaling without equations, modelers generally compare a nonrandom prototype event of significant sediment transport quantity and time duration with model performance. This is not possible with a highly transient model such as dam failure.

Froude scaling applies to the crest hydraulics where friction does not play a significant part. A length ratio, L_r, of 15 was selected to make the 2.12-foot-high (646-mm) model dam represent a typical National Park Service embankment dam about 32 feet high (9.754 m). Thus, by Froude Law:

D_r = 15   depth of flow ratio, prototype-model
q_r = 58.1   unit discharge ratio
Q_r = 871   total discharge ratio
V_r = 3.87   velocity ratio
T_r = 3.87   hydraulic time ratio
R_r = 58.1   Reynolds number distortion ratio

Kamphius [5], also, Brown and Chu [6] show that rugosity, k_s, is two times the d_{90} size of the sediment bed material. Since d_{90} was 2 millimeters, in the model, the k_s simulated by scaling was 60 millimeters. It is expected that the model is too rough and velocities tend to model low and depths high.

Because of the lack of a fully verified transport equations, lack of Froude scaling for shallow flow, the model results are considered qualitative, more likely indicating which treatment of those tested worked better rather than determining actually how much better.

Laboratory Test Facility

A typical National Park Service embankment dam, Blue Ridge Parkway, was represented in the sectional model. The model represented a 32-foot-high (9.754-m) dam and was constructed of materials similar to those of the prototype dam. The model embankment overflow represented about 4 feet (1.219 m) of water overtopping the crest of the dam for a period of 4 to 6 hours. The test embankments were placed in a 3-foot wide by 4-foot deep by 30-foot long (914-mm by 1219-mm by 9144-mm) flume shown on figure 11. The 3-foot flume width represented 45 feet (13.716 m) of crest length. The model dam was 2.12 feet (646 mm) high and the crest extended 1.58 feet (482 mm) in the direction of flow.

Water was supplied to the flume by a portable laboratory pump. Discharges were measured by an 8-inch (203-mm) orifice venturi meter. One side of the flume had windows for viewing erosion and flow action. A nominal 12-inch (300-mm) diameter pipe with a gate valve was used to pass flow around the test embankment. Upon closing the valve, the reservoir water level would rise and flow over the test embankment.

Soil Tested

Soil used for all test runs was a clayey sand found near Denver. The soil had 45 percent fines passing the U.S.A. Standard series No. 200 sieve and 6 percent gravel retained on the No. 4 sieve. The soil gradation curve, shown on figure 12, indicates that the d_{100} size is 19.1 millimeters and the d_{90} size is 1.9 millimeters. The soil has an LL (liquid limit) of 25 percent and a PI (plasticity index) of 9 percent.

Soil was placed and compacted to the desired test density of 95 percent standard Proctor for all but one test. The placement for test run 8 was overcompacted to 102 percent. The moisture compaction–penetration resistance curves for the soil are plotted on figure 13. Soil compaction was controlled by determining the soil mass required to fill 3-inch (76-mm) thick horizontal layers of model embankment soil, and determining the amount of moisture that needed to be added to obtain optimum compaction. To obtain better bonding between layers, the top of each layer was scarified before placing the next layer.

A 6:1 slope was used for early tests because many investigators intuitively believe that this is a rational erosion resistant slope. This was previously discussed in section "Gravity Effects on Erosion Resistance." In later tests, 4:1 slopes were used
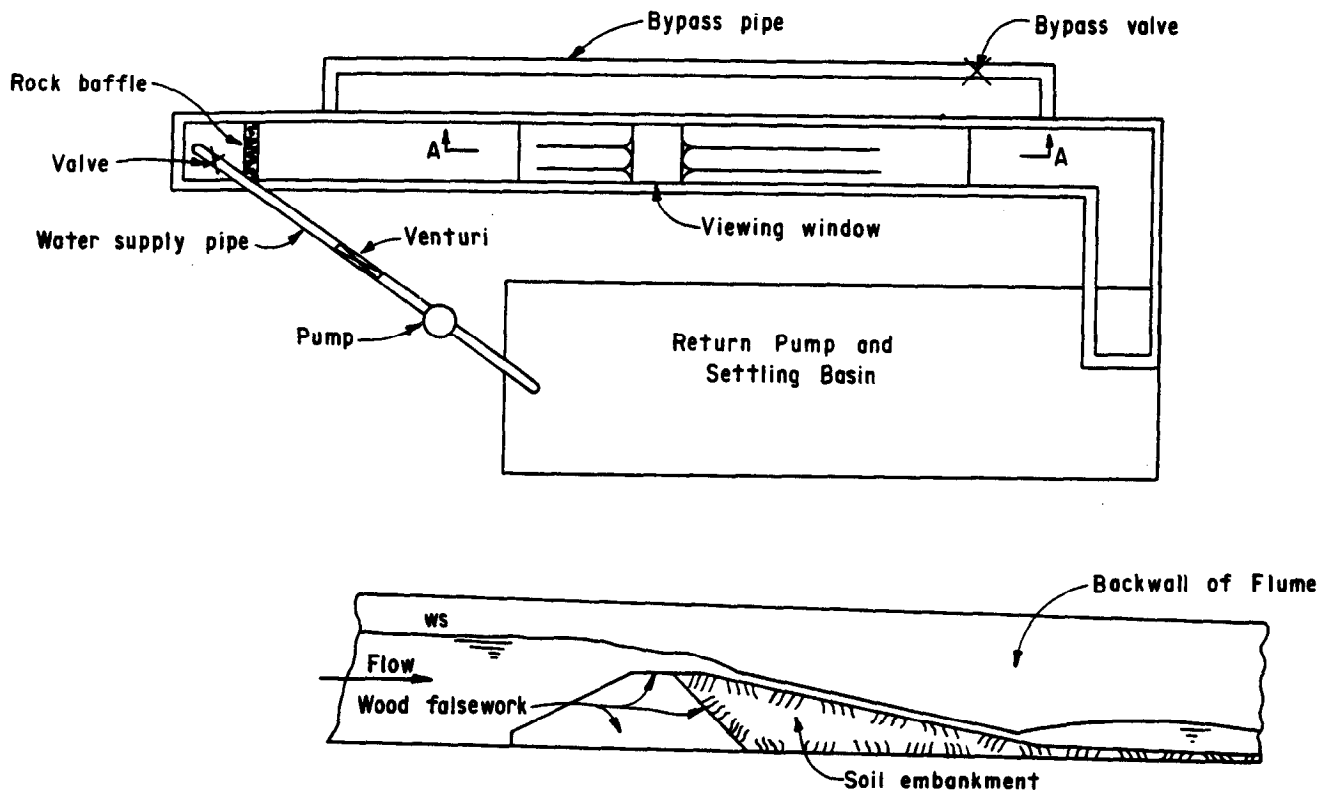
SECTION A-A

Figure 11. – Laboratory test facility.

because of the high stability experienced with tests with gabions.

Model Operation

For most of the nine test arrangements, the unit discharge represented was 40 (ft³/s)/ft [3.716 (m³/s)/m]. The arrangement for test run 7 was replicated for test run 8 but operated at a unit discharge representing 87 (ft³/s)/ft [8.082 m²/s)/m]. The first test run lasted only 17 minutes because erosion was considered to be excessive and more consideration needed to be given to the boundary effects of the model and the smoothness of the hard cap at the crest. Therefore, 17 minutes (about 1-hour prototype time) was used as a common model test run time interval for the remaining tests to compare after erosion measurements. Some test treatments were operated an additional hour which would be representative of 5 hours total of overtopping which is expected for the National Park Service dams being considered for modification. A surveyors level was used to determine bed profiles and cross sections. A prism-end area method was used to calculate erosion volumes.

Description of Slope Treatments Tested

The following are descriptions of embankment treatments tested with run numbers related to schematic sketches in table 5.

Run 1: Hard crest cap.—The crest was protected with a hard cap shown in table 5. The cap extended 10 feet (3.05 m) down the slope and ended with 7-foot (2.13 m) vertical toe curtain. Soil was placed in the model at 95 percent maximum Proctor compaction. Simulated overtopping flow was 40 (ft³/s)/ft [3.716 (m³/s)/m].

Run 2: Fixed cobble roughness on downslope part of crest cap.—Crushed pea-sized gravel roughness was epoxied to the downhill slope of the crest cap. The pea gravel represented rock roughness from 3 to 6 inch (76 to 152 mm) size. The previous tested embankment was excavated beyond the erosion and the soil replaced at 95 percent maximum Proctor density.

Run 3: Downslope riprap.—A 30-foot (9.144 m) slope length of riprap was placed just
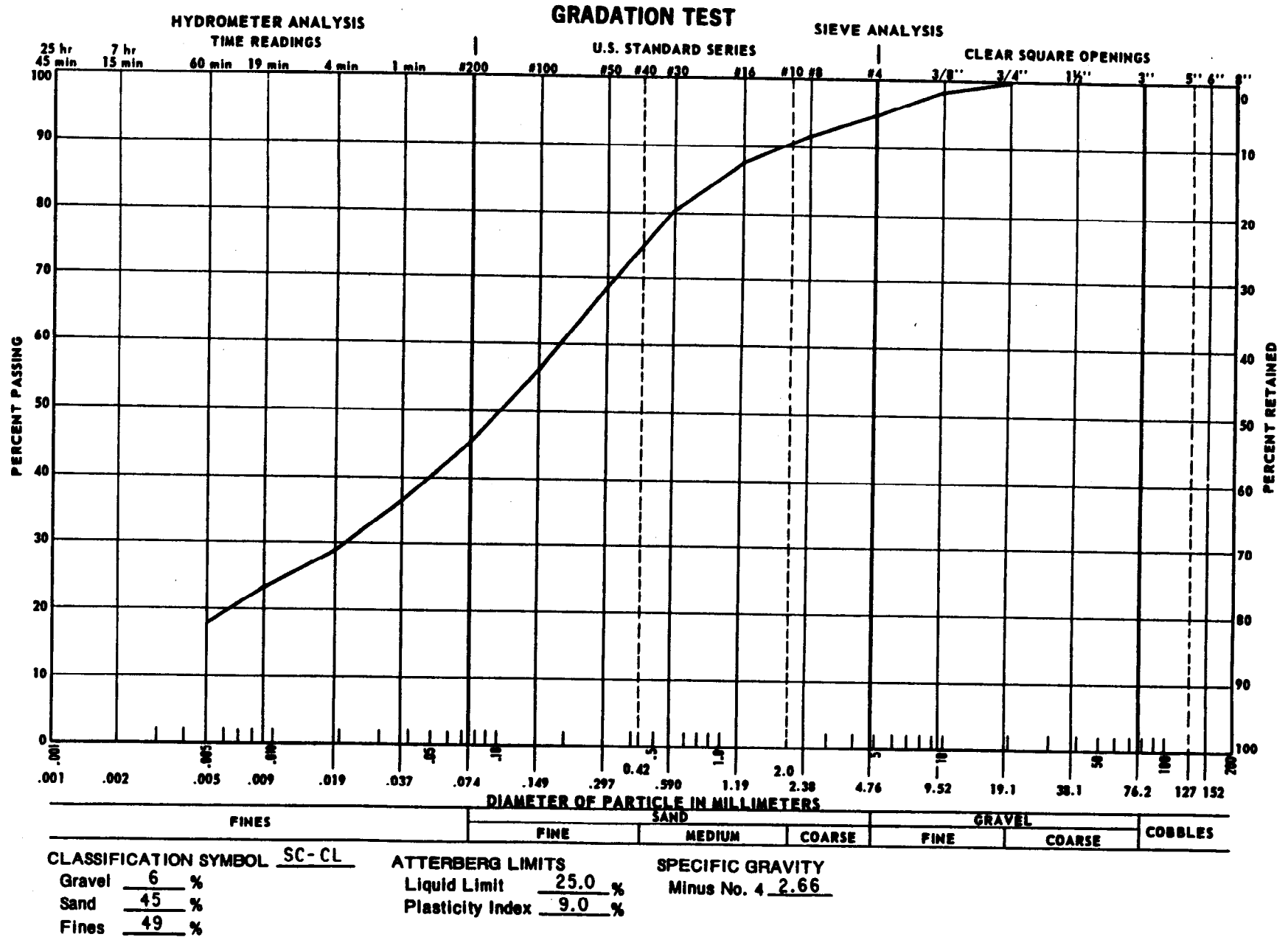
20

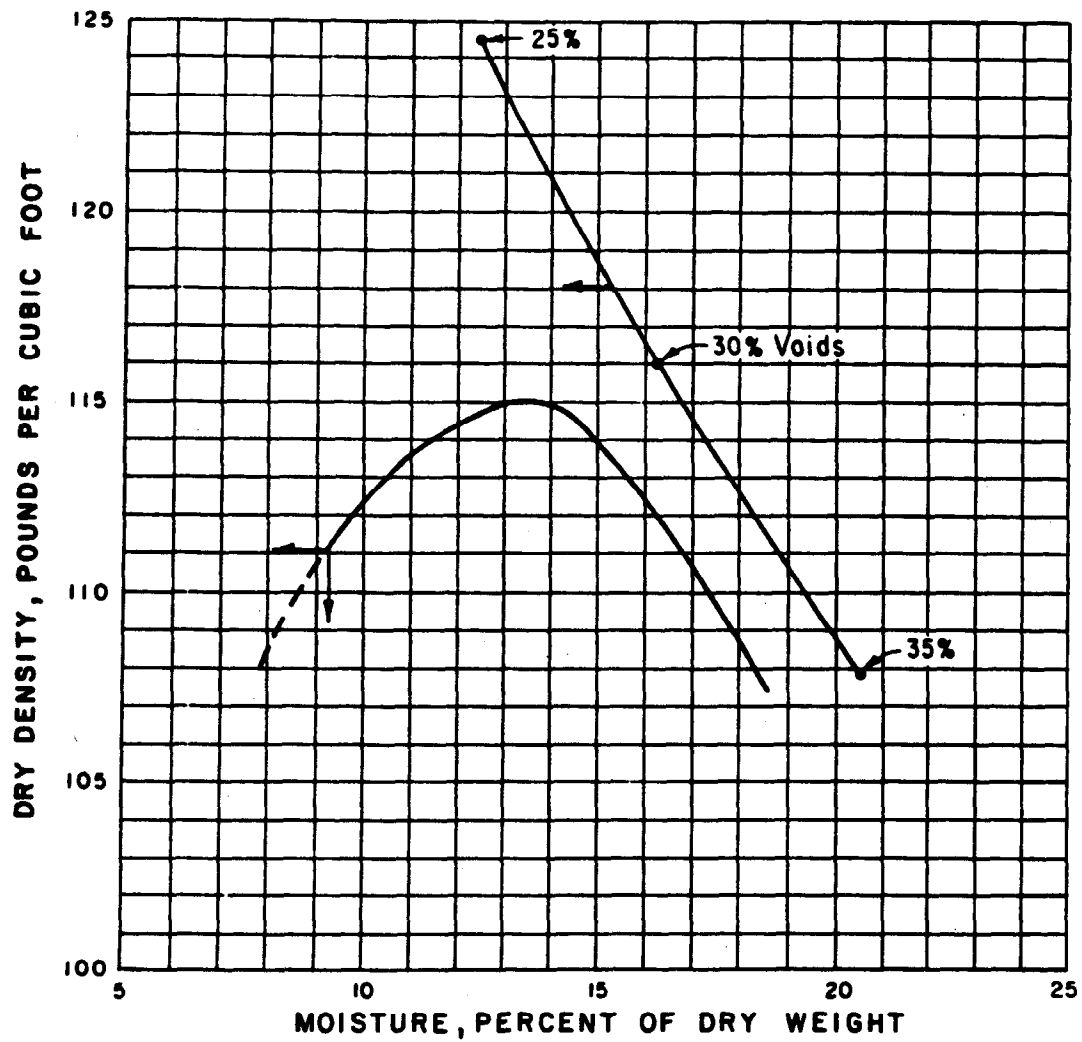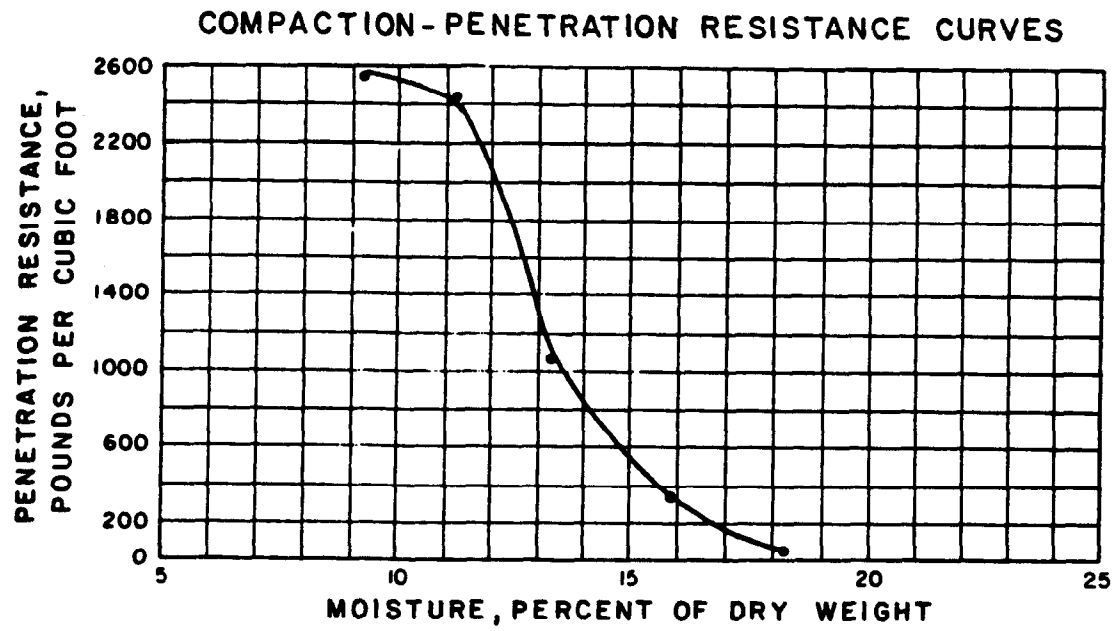Figure 12. — Gradation test of soil used for test runs 1 through 9.

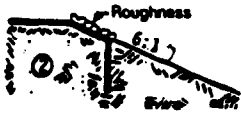# COMPACTION - PENETRATION RESISTANCE CURVES
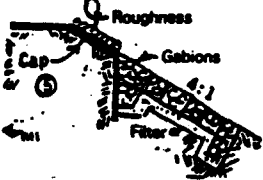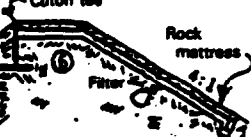
Figure 13. – Compaction–penetration resistance curves.

Table 5. – Results of overtopping flow model—summary.

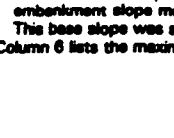| Sketch and run number (1)	Unit discharge, $\frac{ft^3/s}{ft}$ (2)	Elapsed time (3)	Relative volume erosion rate per unit area (Test 7 comparison base), hours (4)	Maximum scour depth°, ft, Scour location (5)	Maximum scour depth,† ft, Scour location (6)
Hard crestcap, Soil — ①	40	1	2.41	-7.5 15.2	10.0 15.2
Roughness — ②	40	1	1.09	0.0 10.1	8.8 106.2
Riprap, Filter — ③	40	1	2.03	-5.9 10.1	8.0 10.1
Gabions — ④	40	1	0.42	8.8 40.6	1.9 83.7
	40	5	0.50	8.1 40.6	3.8 95.1
Roughness, Cap, Gabions, Filter — ⑤	40	1	2.19	-1.3 52.8	3.4 59.2
Cutoff toe, Rock mattress, Filter — ⑥	40	1	0.94	3.8 59.2	6.3 104.3
	40	5	0.63	2.5 83.7	10.0 83.7
— ⑦	40	1	1.00	-0.3 0.0	5.0 77.3
95% Compaction Standard Proctor	40	5	1.00	-2.5 0.0	8.8 59.2
Soil — ⑧	87	1	2.02	-0.3 0.0	3.8 toe
102% Compaction Standard Proctor	87	5	0.00	-0.9 0.0	5.6 toe
— ⑨ 95% Compaction Standard Proctor	87	1	1.42	-1.2 0.0	3.4 toe

NOTE: 1 ft = 0.3048 m   1 ft/s = 0.3048 m/s   1 ft³/s = 0.02831 m³/s

°Column 5 lists the depth of embankment soil cover or erosion below an imaginary 2.5:1 slope line and distance down the finished embankment slope measured from the downstream edge of the crest top. Negative values indicate scour below the 2.5:1 line. This base slope was selected because it is typical of Bureau embankment dams that are not rock protected.
†Column 6 lists the maximum scour depth relative to the finished embankment slope and its location on the slope.

downstream of the cobble roughened sloping part of the crest cap. The model riprap represented about 6 to 24 inch (152 to 610 mm) prototype riprap. An appropriate filter base was placed underneath to prevent embankment material from leaching through the riprap.

Run 4: Gabions.—Gabions were placed on the 6:1 slope; 30 feet (9.14 m) long starting at the end of the cobble roughened downstream sloping part of the crest cap. The upstream compartments were securely anchored to the vertical curtain wall of the cap with epoxy. Flexible hook rug backing was used to model the mesh. The model represented 3- by 3- by 3-foot (0.914- by 0.914-by 0.914-m) gabion compartments. The gabions were further anchored to buried timbers in the embankment.

Run 5: Gabions with slope increased.—Because of the success in the previous test, it was decided to try gabions on a 4:1 slope.

Run 6: Rock mattress.—An 18-inch-thick (457-mm) mesh contained rock mattress was anchored to tee-shaped cutoff wall at the upstream corner of the flat part of the crest, covering the flat part of the crest and extending 50 feet (15.24 m) down the downstream 4:1 sloping face of the bank. The vertical leg of the tee extended 6 feet (1.83 m) below the flow boundary. The buried base of the tee was 5 feet (1.52 m) long. For this run only, the model soil on the 3:1 sloped approach was protected with an 18-inch layer of 9-inch maximum and 4-inch mean diameter riprap (457-, 229- and 102-mm respectively).

Runs 7, 8, and 9: Plain soil.—For these three tests 35 feet (10.7 m) of the approach 3:1 slope, the flat part of the crest, and all of the 4:1 slope of the downstream bank were formed with the soil. For test 8, overtopping flow was about 87 (ft³/s)/ft [8.1 (m³/s)/m]. The erosion volume was unexpectedly low compared to that for 40 (ft³/s)/ft [3.7 (m³/s)/m]. A soil test indicated a 102 percent maximum Proctor density rather than the 95-percent target density. Because of the overcompaction for the test 8, the embankment was reformed at 95 percent of Proctor maximum and overtopped at 87 (ft³/s)/ft for run 9.

Results

Two bed scour profiles (examples) are given on figure 14. The top profile is run 7 which was with plain soil embankment and without protective treatment effort other than compaction. The erosion volumes—determined from run 7—were used as base quantities to compare and normalize erosion volumes of the

other runs. The available erodible length for run 7 was considered to begin at the upstream end of the 3:1 approach soil slope and end at the downstream toe of the 4:1 embankment slope. The bottom profile is run 5 which had the cobble roughened crest cap slope with downstream gabion protection. The available erodible length for run 5 was considered to begin at the downstream end of the gabion cover.
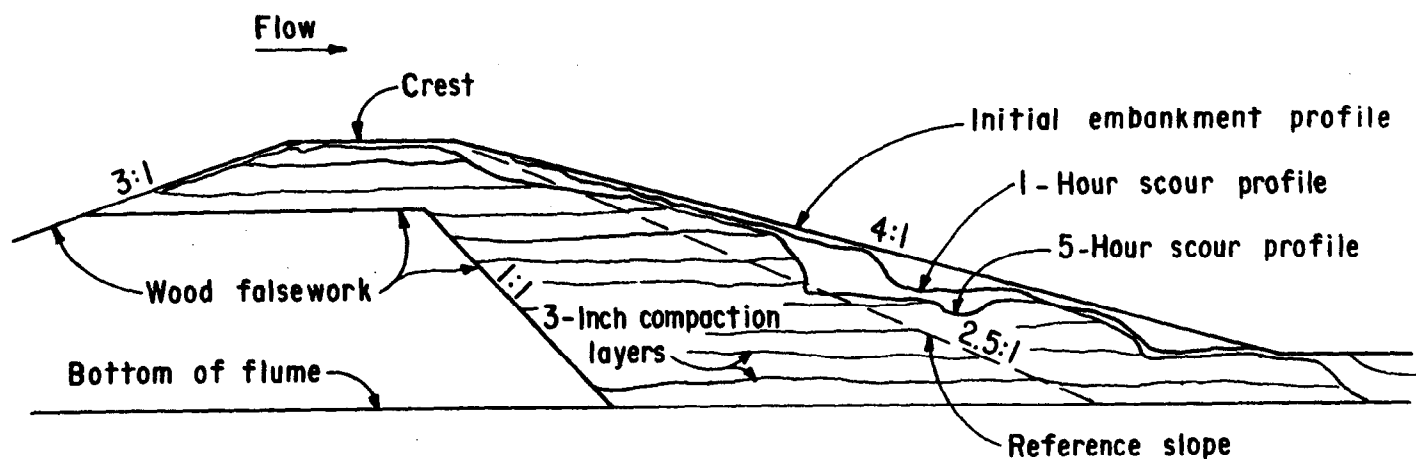
Table 5 contains sketches of the embankment treatments tested and a summary of model results.

- Column 1 shows the downstream slope sketches and test run numbers (circled).
- Column 2 lists the unit discharge being simulated.
- Column 3 notes the total elapsed time of operation before total erosion volume measurement.
- Column 4 lists the relative volume erosion rate per unit area along the erodible embankment length using run 7 as a comparison base.
- Column 5 lists the depth of embankment soil cover or erosion below an imaginary 2.5:1 slope line and distance down the finished embankment slope measured from the downstream edge of the crest top. Negative values indicate scour below the 2.5:1 line. This base slope was selected because it is typical of Bureau embankment dams that are not rock protected.
- Column 6 lists the maximum scour depth relative to the finished embankment slope and its location on the slope.
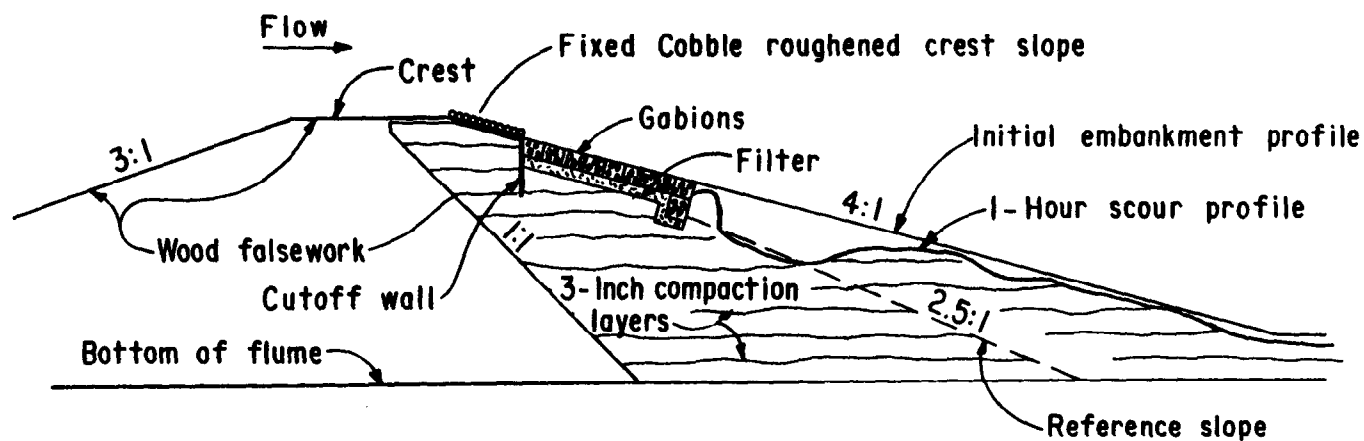
Following are results and implications noted during the studies, tempered with experience from other sediment model studies and conversation with investigators experienced with overtopping occurrences, and review of literature.

During test run 1, with a 6:1 slope, flow rapidly transformed into a chute and pool mode. This type of flow is initiated by shallow bank surface waviness or by jets and eddies caused by flow around and over isolated projecting rocks in the fill material. Brush and trees would also cause local areas of increased scour. Scour holes tended to lift flow resulting in intermediate areas of less scour between areas of increased plunging flow scour. Road pavements, curbs, parapets, and bulging or sagging of top faces of gabion compartments can initiate and affect location and amount of scour.

During test run 1, the smooth vertical walls of the model appeared to exaggerate scour, with deep holes in the embankment near the flume walls and the vertical curtain wall of the hard protective crest cap. Reservoir grain roughness and larger geometric bed form perturbations cause eddies that follow the flow over the upstream slope of the dam and stretch out parallel to the bed and intensify into vortices.

24

Flow →

Crest

Initial embankment profile

1-Hour scour profile

5-Hour scour profile

3:1

4:1

Wood falsework

1:1

3-Inch compaction layers

2.5:1

Bottom of flume

Reference slope

(a) Embankment scour for run 7 used as base for run comparisons.

Flow →

Crest

Fixed Cobble roughened crest slope

Gabions

Filter

Initial embankment profile

1-Hour scour profile

3:1

4:1

Wood falsework

1:1

Cutoff wall

3-Inch compaction layers

2.5:1

Bottom of flume

Reference slope

(b) Embankment scour for run 5.

Figure 14. – Typical scour of test embankment.

These vortices can cause local areas of relatively more intense bed shear. Some of the apparent wall effect may have been caused by upflow intensification. Crest end treatments not tested during these studies that contract the flow sideways would also cause vortices that would intensify local scour.

Generally, when flow passes a fixed bed to a soil bed or vice versa, scour occurs. This is caused by small boundary layer disturbances that form as flow adjusts to abrupt changes in boundary roughness. An example of this type of scour is going from the hard crest cap to soil (test run 1). For test run 2, pea gravel was epoxied to the downstream sloping part of the hard crest cap simulating 3 to 6 inch (76 to 152 mm) cobble roughness increasing flow depth and dampening vortex action. This increase in roughness may have contributed to the significantly less, about one-half the erosion volume along available embankment length and the more uniform scour compared to test run 1. This effect also occurs for flow making the transition from gabions to soil.

Despite the previously discussed modeling limitations, velocity, depth, and discharge were scaled by Froude Law for comparison purposes. The scaled velocity for all test runs rapidly reached more than 30 ft/s (9.144 m/s). The general riprap design methods compared in reference [34] do not account for the combination of high velocity, steep downslope flow, nor shallow flow because they use uniform flow equations and entrainment functions developed empirically from uniform flow data. During test run 3, model riprap representing 6 to 24 inch-diameter (152 to 610 mm) stones became fluidized and eroded out immediately.

Gabions and mattress pods were modeled for test runs 4, 5, and 6. They were represented by cages or compartments formed with 4-inch (102-mm) mesh materials filled with angular rock up to 12-inch (305-mm) maximum diameter and placed on a filter bed. During these tests, there was no indication that the gabions or mattress pods would be dislodged by the overtopping flow. It could not be determined if the embedded anchors were needed for the stability demonstrated. However, the author is unaware of manufacturer data for velocities greater than about 24 ft/s (7.3 m/s). As stated previously, the modeled velocities greater than 30 ft/s (9.144 m/s) occurred on the slope for all tests. On the 4:1 slope the main erosion was near the downstream end of the protection. Whereas, for the 6:1 slope the main scour hole was 36 feet (10.973 m) farther downstream. Comparing test runs 4 and 5 indicates that the effect of increasing the downslope from 6:1 to 4:1 increased the scour volume about five times. However, the maximum depth of scour was about 1-¾ times deeper. A minor part of the different scour locations

can be attributed to sagging and bulging of gabion compartment tops.

Erosion data for the 5-hour test runs were used to observe if the rough flow later in the test had a greater or less transport rate than the earlier smooth flow. For these tests, the sediment transport rate for the last 4 hours averaged about one-fourth of the rate for the first hour. Thus, it appears that the chute and pool mode flow reduced erosion relative to earlier smooth flow erosion. The percent of total volume eroded, computed from survey levels, did not significantly increase during the last 4 hours of test run 8. Possibly, not enough elevation measurements or cross sections were obtained with a surveyor's level.

Model test results, of runs 8 and 9, having similar protective treatment, indicate that increasing standard Proctor compaction from 95 to 102 percent density reduced erosion by one-half.

Comparing results of test runs 7 and 9 showed that increasing unit discharge from 40 to 87 (ft³/s)/ft [3.716 to 8.083 (m³/s)/m] resulted in about 40-percent increase in erosion.

Despite exercising care during field construction and inspection, low areas always exist along a dam crest. Low areas can occur after construction because of crest traffic, nonuniform settling, and lack of maintenance. Erosion mode at a low point on the crest could depend on the shape of hydrograph during overtopping. For example, with slow rising or low constant flow, the erosion may start and remain at one low point causing gulley type erosion, continuing on to breaching. If flow rose fast enough, the effect of a low area could be drowned out and result in sheet flow erosion.

The reservoir overflow head on the crest should not be greater than about one-third the crest length in the direction of flow. This would cause a flow cavity at the upstream end of the crest. When head is less than about one-twelfth the crest length, friction affects flow considerably, undulation occurs and depth can approach critical more than once. Long-term flows outside the limit equation (12) increases risk of scour on the top of the crest.

OTHER POSSIBLE TREATMENTS NOT TESTED

Other possible treatments for downstream slope protection were discussed during meetings or found in the literature search. Some of these are expensive—material wise and labor intensive—but still

could be possible alternatives for treating existing small embankment dams. Possible treatments are:

1. Plastic sheets with thin expendable soil cover to protect them from ultraviolet and other physical damage. Another suggestion was plastic sheets rolled up under protective hoods and arranged so flow would roll them down the slope when needed. It is possible that general bank waviness could rapidly cause rippling or undulation of the plastic sheets resulting in tearing destruction.

2. Existing spillway capacity can be increased by hooding them so as to take advantage of additional head caused by siphon effect. The siphon must be designed properly to regulate air. Ervine [35] shows an example head—discharge curve for air regulated siphons. All or part of a spillway could be made into a siphon depending upon additional discharge needed. This method may be too costly.

3. Flow through and over mesh contained rock weirs and dams have been used and reported by Australians and New Zealanders. A summary of their experiences and references are given by Thomas [36].

4. Reeves [37] discusses the use and economy of using roller-compacted concrete to permit overtopping flow.

5. The U.S.S.R. developed protective blocks that interlock and cause negative pressure underneath them so that they are increasingly sucked onto the embankment filter as flow velocity increases. Smith [38] model tested and concluded ". . . that the compressive soil strength was the only limit to protection provided by the blocks."

6. Another suggestion was the possibility of lifting the flow just below and near the crest to flip it to a downstream scour area of less threat to the embankment.

BIBLIOGRAPHY

[1] Powledge, G.R., and R.A. Dodge, "Overtopping of Small Dams—An Alternative for Dam Safety," Hydraulics and Hydrology in the Small Computer Age, American Society of Civil Engineers Specialty Conference, August 1985.

[2] Miller, S.P., M. Hon-Yim Ko, and J. Dunn, "Embankment Overtopping," Hydraulics and Hydrology in the Small Computer Age, American Society of Civil Engineers Specialty Conference, August 1985.

[3] Smerdon, E. T., and R. P. Beasley, "The Tractive Force Theory Applied to Stability of Open Chan-nels in Cohesive Soils," Research Bulletin 715, University of Missouri, 1959.

[4] Rouse, H., Elementary Mechanics of Fluids, Wiley, 1946.

[5] Kamphuis, J.W., "Determination of Sand Roughness for Fixed Beds," Journal of Hydraulic Research vol. 12, No. 2, 1974.

[6] Brown, B.J., and Y.H. Chu, "Boundary Effects of Uniform Size Roughness Elements in Two-dimensional Flow in Open Channels," Miscellaneous Paper H–68–5, Corps of Engineers, Waterways Experiment Station, Vicksburg, Missisipppi, 1968.

[7] Bathurst, J.C., R.M. Li, and D.B. Simons, "Resistance Equation For Large-scale Roughness," Journal of Hydraulic Engineering, HY12, American Society of Civil Engineers, December 1981.

[8] Knight, D.W., and H.S. Patel, "Boundary Shear in Smooth Rectangular Ducts," Journal of Hydraulic Engineering, vol. III, No. 1, January 1985.

[9] Bos, M.G., "Discharge Measurement Structures," Publication 20, ILRI, Delft Hydraulics Laboratory, The Netherlands, 1976.

[10] King, H.W., "Handbook of Hydraulics," 3d ed., McGraw-Hill Book Co., Inc., 1939.

[11] Schlicting, "Boundary Layer Theory," Pergamon Press, 1955.

[12] Jacobs, W., "Umformung Eines Turulenten Geschwindigkeits—Profiles," ZAMM, 19, 87–100, 1939.

[13] Gibbs, H.J., "A Study of Erosion and Tractive Force Characteristics in Relation to Soil Mechanics Properties," Bureau of Reclamation Report No. EM–643, 1962.

[14] Carlson, E.J., and P.F. Enger, "Studies of Tractive Forces of Cohesive Soils in Earth Canals," Bureau of Reclamation Report No. Hyd–504, 1962.

[15] Lane, E.W., "Progress Report on the Design of Stable Channels," Bureau of Reclamation Report No. Hyd–352, 1952.

[16] Kelly, W.E., and R.C. Gularte, "Erosion Resistance of Cohesive Soils," American Society of Civil Engineers, HY10, 1981.

[17] Kamphius, "Cohesive Material Erosion by Unidirectional Current," Journal of Hydraulic Engineering, vol. 109, No. 1, January 1983.

[18] Simons, D.B., and F. Senturk, "Sediment Transport Technology," WRP, Fort Collins, Colorado, 1977.

[19] Shields, A., "Application of Similarity Principles and Turbulence Research to Bedload Movement," Translation CIT, Pasadena, California, 1936.

[20] Krishnamurthy, M., "Incipient Motion of Cohesive Soils," American Society of Civil Engineers Specialty Conference, Frontiers of Hydraulic Engineering, August 1981.

[21] Carlson, E.J., "Critical Tractive Forces on Channel Side Slopes in Coarse Noncohesive Material," Bureau of Reclamation Report No. Hyd–366, 1966.

[22] Brooks, N.H., Discussion, Journal of The Hydraulics Division, American Society of Civil Engineers, vol. 87, No. HY3, Proc. Paper 3529, May 1963.

[23] Simons, D.B., "Theory and Design of Stable Channels in Alluvial Material," Ph.D. Dissertation, Colorado State University, Fort Collins, Colorado, 1957.

[24] Gessler, Johannes, "The Beginning of Bedload Movement of Mixture Investigated as Natural Armoring in Channels," Translation T–5, Keck Laboratory, California Institute of Technology, October 1968.

[25] Graf, W.H., and G.C. Pazis, "Les Phenomenes de Deposition et D'erosion Dans un Canal Alluvionnaire," Journal of Hydraulic Research, vol. 15/2, 1977.

[26] Vanoni, V.A., "Sedimentation Engineering," American Society of Civil Engineers, Manuals and Reports on Engineering Practices, No. 54, 1975.

[27] Metha, A.J., T.M. Parchure, J.G. Dixit and R. Ariathurai, "Resuspension Potential of Deposited Cohesive Sediment Beds," Estuarine Comparisons, Academic Press, 1982.

[28] Kandiah, A., "Fundamental Aspects of Surface Erosion of Cohesive Soils," Ph.D. Thesis, University of California, Davis, 1974.

[29] Chen. Y.H., "Embankment Overtopping Test to Evaluate Damage," American Society of Civil Engineers Specialty Conference, Hydraulic and Hydrology in the Small Computer Age, Lake Buena Vista, Florida, August 1985.

[30] Ariathurai, R., and K. Arulanadan, "Erosion Rates of Cohesive Soils," Journal of Hydraulics Division, American Society of Civil Engineers, vol. 104, No. HY2, February 1978.

[31] Klein, S.J., "Similitude and Approximation Theory," McGraw-Hill Book Company, Inc., 1965.

[32] Bagnold, R.A., "Sediment Discharge and Stream Power—A Preliminary Announcement," USGS Circular 421, 1960.

[33] Abt, S.R., and J.F. Ruff, "Estimating Culvert Scour in Cohesive Material," Journal of Hydraulics Division, American Society of Civil Engineers, vol. 108, HY1, January 1982.

[34] Dodge, R.A., and C.J. Orvis, "Model Study and Riprap Design for Columbia River," ASCE Specialty Conference, Water Forum '81, Waterway Port, Coastal and Ocean Division, vol. II, August 1981.

[35] Ervine, D.A., "The Design and Modeling of Air-regulated Siphon Spillways," Proceedings, I.C.E.., Part B2, B.H.R.A., May 1975.

[36] Thomas, H.H., "Flow Through and Over Rockfill, Engineering for Large Dams," part II, Wiley Interscience Pub., 1976.

[37] Reeves, G.N., "Planned Overtopping of Embankments Using Roller Compacted Concrete," American Society of Civil Engineers Specialty Conference, Hydraulics and Hydrology in the Small Computer Age, Lake Buena Vista, Florida, August 1985.

[38] Smith, K.V.H., "Hydraulic Modeling of Materials for Protecting Earth Weirs," International Conference, Hydraulic Modeling of Civil Engineering Structures, Coventry, England, September 1982.